Heterogeneous endocrine cell composition defines human islet functional phenotypes

AUTHORS

Carmella Evans-Molina[1,2,3,4,5,6,7,18*], Yasminye D. Pettway[8,18], Diane C. Saunders[9,18], Seth A. Sharp[10,18], Thomas SR. Bate[9], Han Sun[10], Heather Durai[9], Shaojun Mei[9], Anastasia Coldren[9], Corey Davis[9], Conrad V. Reihsmann[9], Alexander L. Hopkirk[9], Jay Taylor[9], Amber Bradley[9], Radhika Aramandla[9], Greg Poffenberger[9], Adel Eskaros[9], Regina Jenkins[9], Danni Shi[11], Ke Xu[11], Hakmook Kang[11], Varsha Rajesh[10], Swaraj Thaman[10], Fan Feng[9], Jean-Philippe Cartailler[12], Alvin C. Powers[8,9,13], Kristin Abraham[14], Anna L. Gloyn[10,15,16*], Joyce C. Niland[17*], and Marcela Brissova[9,19*] on behalf of the Integrated Islet Distribution Program

AUTHOR AFFILIATIONS AND FOOTNOTES

Departments of [1]Pediatrics, [2]Medicine, [3]Anatomy, Cell Biology, and Physiology, and [4]Biochemistry and Molecular Biology, the [5]Center for Diabetes and Metabolic Diseases, and the [6]Herman B. Wells Center for Pediatric Research, Indiana University School of Medicine, Indianapolis, IN 46202, USA

[7]Richard L. Roudebush VA Medical Center, Indianapolis, IN 46202, USA

[8]Department of Molecular Physiology and Biophysics, Vanderbilt University School of Medicine, Nashville, TN 37232, USA

[9]Division of Diabetes, Endocrinology, and Metabolism, Department of Medicine, Vanderbilt University Medical Center, Nashville, TN 37232, USA

[10]Department of Pediatrics, Stanford School of Medicine, Stanford, CA 94305, USA

[11]Department of Biostatistics, Vanderbilt University Medical Center, Nashville, TN 37232, USA

[12]Vanderbilt Center for Stem Cell Biology, Vanderbilt University, Nashville, TN 37232, USA

[13]VA Tennessee Valley Healthcare System, Nashville, TN 37232, USA

[14]Division of Diabetes, Endocrinology, & Metabolic Diseases, National Institutes of Health, Bethesda, MD 20892, USA

[15]Department of Genetics, Stanford School of Medicine, Stanford, CA, USA

[16]Stanford Diabetes Center, Stanford School of Medicine, Stanford, CA, USA

[17]Department of Diabetes and Cancer Discovery Science, Arthur Riggs Diabetes and Metabolism Research Institute, Beckman Research Institute, City of Hope, Duarte, CA 91010, USA

[18]These authors contributed equally

[19]Lead Contact

*Corresponding Authors (in alphabetical order)

Address correspondence and requests for reprints to: Marcela Brissova, marcela.brissova@vanderbilt.edu; Carmella Evans-Molina, cevansmo@iu.edu; Anna L. Gloyn, agloyn@stanford.edu; and Joyce C Niland, jniland@coh.org

SUMMARY

Phenotyping and genotyping initiatives within the Integrated Islet Distribution Program (IIDP), the largest source of human islets for research in the U.S., provide standardized assessment of islet preparations distributed to researchers, enabling the integration of multiple data types. Data from islets of the first 299 organ donors without diabetes, analyzed using this pipeline, highlights substantial heterogeneity in islet cell composition associated with hormone secretory traits, sex, reported race and ethnicity, genetically predicted ancestry, and genetic risk for type 2 diabetes (T2D). While α and β cell composition influenced insulin and glucagon secretory traits, the abundance of δ cells showed the strongest association with insulin secretion and was also associated with the genetic risk score (GRS) for T2D. These findings have important implications for understanding mechanisms underlying diabetes heterogeneity and islet dysfunction and may provide insight into strategies for personalized medicine and β cell replacement therapy.

KEYWORDS

Human islets, alpha cells, beta cells, delta cells, insulin secretion, glucagon secretion, T1D, and T2D genetic risk score

INTRODUCTION

Diabetes mellitus impacts over 11% of Americans and is the eighth leading cause of death in the U.S., with an estimated economic cost of over $413 billion annually[1,2]. Type 1 diabetes (T1D) accounts for 5-10% of all diabetes cases and results from autoimmune-mediated destruction and loss of the insulin-producing β cells, whereas type 2 diabetes (T2D), the most prevalent diabetes form, is characterized by β cell dysfunction and peripheral insulin resistance. While the etiologies of T1D and T2D are largely distinct, both forms require loss and/or dysfunction of pancreatic β cells, have a strong genetic component, and are heterogeneous regarding disease pathophysiology, progression, and response to therapeutic interventions [3–7]. Increasingly, data from clinical cohorts, tissues derived from human organ donors and mouse models highlight a role for impaired function of other islet cell subtypes, including α cells and δ abnormalities in diabetes pathophysiology[8–18]. Murine models have advanced our understanding of disease pathophysiology; however, there are critical differences in the function and architecture of murine and human pancreatic islets necessitating the comprehensive study of human islets to translate basic science research findings[19–25].

The Integrated Islet Distribution Program (IIDP), formerly the Islet Cell Resource[26], has served as the main source of human islets for research within the U.S., with nearly 300 million islets supplied for use in more than 600 unique studies to date (https://iidp.coh.org/). Located at City of Hope (Duarte, CA) and funded by the National Institutes of Diabetes and Digestive and Kidney Diseases (NIDDK) with targeted programmatic funding from Breakthrough T1D (formerly JDRF), the IIDP's mission is to distribute high-quality human islets to the diabetes research community to support basic science and translational research. The IIDP subcontracts with a group of expert islet isolation centers at institutions across the country, who procure donated pancreata from their local Organ Procurement Organizations (OPOs). Rigorous protocols are followed to isolate the islets while maximizing the yield, viability and purity. An automated algorithm developed by the IIDP ensures fair and equitable islet distribution, matching the islet offers to awaiting researchers who have subscribed to receive islets and other non-islet biospecimens from the IIDP[27,28].

In response to the NIH's call to enhance rigor, reproducibility, and transparency in biomedical research, the IIDP initiated the Human Islet Phenotyping Program (HIPP) at Vanderbilt University Medical Center and the Human Islet Genotyping Initiative (HIGI) Program at Stanford University to provide systematic phenotypic and genotypic assessment of IIDP-supported human islet preparations (**Extended Data Figure 1**)[29]. This workflow comprehensively evaluates islet morphology, purity, and viability (**Extended Data Figure 2**). For

the first time, it also assesses islet cell composition and concurrently examines the *in vitro* β and α cell function[12,30–35]. It also generates the genetic risk scores (GRS) for T1D and T2D while predicting genetic ancestry across a diverse group of organ donors in the U.S. (see **Figure 1A**). This centralized approach reduces redundancy and provides cost savings to investigators to accelerate the speed of scientific discoveries made using these islets. Importantly, the IIDP provides this rich integrated islet data generated by the HIPP and HIGI for researchers to explore via the online IIDP Research Data Repository (RDR). Here, we present an analysis of the first 299 IIDP-supported islet preparations from donors without a clinical diagnosis of diabetes analyzed using the HIPP and HIGI pipelines. Our integrated analysis of this dataset highlights marked heterogeneity in islet secretory traits and points to a previously underappreciated heterogeneity in islet cell composition. We found that the heterogeneity concerning three primary endocrine cell types, α, β, and δ cells, is associated not only with islet hormone secretion traits but also with sex, reported race and ethnicity, genetically predicted ancestry, and T2D GRS. While α and β cell composition influenced insulin and glucagon secretory traits, most notably, the abundance of a relatively small δ cell population showed the strongest association with insulin and glucagon secretion traits. Delta cell composition was also associated with the T2D GRS. These findings have important implications for understanding the mechanisms underlying personalized signatures—whether genetic, functional, or architectural—that predispose individuals to diabetes. Additionally, they may influence the progression and treatment outcomes of the disease, as well as inform β cell replacement therapy using human islets for transplantation.

RESULTS

We present an analysis of the first release of 299 human islet preparations from donors without diabetes, for which all relevant donor information was available (**Figure 1B**). This dataset was derived from a diverse pool of donors with respect to reported race, ethnicity, age, and BMI. Islets from male donors were overrepresented in the dataset (62%), which is reflective of overall trends in available islets and organ donors in the U.S.[36]. The distribution of reported race or ethnicity differed between male and female donors ($p = 0.014$), where the dataset included a higher percentage of female donors that were reported Black or African American (15% vs. 5%, $p = 0.006$). A higher percentage of male donors were Hispanic or Latino, though this difference was not statistically significant). In 90% of the human islet preparations for which genotyping data was available, the genetic ancestry of the donor was predicted ($n = 268$; **Figure 1C**). Overall, there was a high concordance between reported race or ethnicity and primary predicted

genetic ancestry within the two datasets ($\kappa = 0.867$, $p < 0.001$). Similar to the larger dataset, there was a lower percentage of male donors with primary African ancestry (2.5% vs. 16%, $p = 0.0002$) and a higher proportion of male donors with Admixed American ancestry (38.5% vs. 22%, $p = 0.009$).

Demographic features were similar in the group of donors where genetic ancestry was predicted (**Figure 1B-C**). There were no significant differences in age, BMI, or HbA1c between male and female donors by Wilson rank sum test. The mean age of male and female donors was 43 (range 15 – 68 years) and 46 years (range 20 – 65 years), and BMI averaged 29 kg/m^2 in both male (range 13.7 – 46.8 kg/m^2) in female donors (range 17.6 – 47.6 kg/m^2). The mean HbA1c of male and female donors was 5.4% (range 4 – 6.3%) and 5.3% (range 4.3 – 6.4%). Of note, this dataset includes islets from donors within a normal HbA1c range, defined by the American Diabetes Association as <5.7% (n = 223, mean ± SD: 5.2 ± 0.3, range 4.0 – 5.6), as well as a subset of islets from donors with an HbA1c ≥ 5.7% (n = 76, mean ± SD: 5.9 ± 0.2, range 5.7 – 6.4). Together, these data form a powerful dataset to understand population-based differences in human islet phenotype.

Islet processing traits associated with islet purity and viability

IIDP-affiliated islet isolation centers identify, process donor pancreata, and distribute human islet preparations for phenotypic assessment by the HIPP, genotypic assessment by the HIGI, and scientific investigation by researchers (**Supplemental File 1**). The IIDP RDR includes data on islet purity and viability, which are measured by islet isolation centers and made available to researchers at broadcast (i.e., prior to distribution, at the time the islets are offered to investigators). The post-shipment islet purity and viability is assessed by the HIPP on the day of arrival. The RDR also includes data related to islet processing, including organ cold ischemia duration, pre-shipment culture time, and transit time. The current dataset included human islet preparations from five islet isolation centers: Scharp-Lacy Research Institute (n = 113), Southern California Islet Cell Resource Center (n = 94), University of Miami Diabetes Research Institute (n = 30), University of Pennsylvania Islet Transplant Center (n = 21), and the University of Wisconsin Human Islet Core (n = 35). Pre-shipment culture time averaged 57.5 hours (range 8 – 237 hours), and the average transit time to the HIPP was 25 hours (range 10 – 102 hours). The mean islet purity measured by the HIPP was 73% (range 15 – 95%), and the mean dispersed islet cell viability was 76% (range 43 – 93%). Islet transit time and dispersed cell viability were positively correlated (Spearman $r = 0.2$, unadjusted p-value (p_{unadj}) = 0.001,

100 **Extended Data Figure 3**). The HIPP assessment of islet purity did not show an association with
101 cold ischemia duration, pre-shipment culture time, or islet transit time.

102 ***Islet secretory function is highly heterogeneous amongst donors***

103 A dynamic perifusion system was used to investigate simultaneously β and α cell
104 hormone secretion in response to both physiologic and pharmacologic stimuli with co-
105 stimulatory and opposing effects on insulin and glucagon secretion. This included basal glucose
106 (5.6 mM), high glucose (16.7 mM), high glucose with isobutylmethylxanthine (IBMX), low
107 glucose (1.7 mM) with adrenaline (Ad), and potassium chloride (KCl). On average, high glucose
108 led to a 7.9-fold increase in stimulated insulin secretion and inhibited glucagon secretion by 0.4-
109 fold on average compared to basal glucose. In contrast, low glucose with adrenaline led to the
110 opposite effect, reducing insulin secretion by approximately 0.2-fold and increasing glucagon
111 secretion by 5.1-fold compared to basal glucose. Exposure to IBMX, a phosphodiesterase
112 inhibitor that increases intracellular cAMP levels, potentiated glucose-stimulated insulin
113 secretion (14-fold) and stimulated glucagon secretion (6.5-fold) compared to basal glucose
114 level. Additionally, KCl-induced membrane depolarization potently stimulated both insulin and
115 glucagon secretion by approximately 31- and 11-fold on average, respectively (**Figure 2A-B**).

116 To understand how biological variables and islet processing features impacted hormone
117 secretion across donors, we derived 11 insulin and 9 glucagon secretion traits from the
118 respective hormone secretion traces (**Figure 2C-D**). For each human islet preparation, we
119 derived the following secretion traits from each insulin trace: basal insulin secretion, glucose-
120 stimulated 1st phase secretion (G 16.7 1st area under the curve; AUC), glucose-stimulated 2nd
121 phase secretion (G 16.7 2nd phase secretion), overall glucose-stimulated insulin secretion (G
122 16.7 AUC), the glucose stimulation index (SI; G 16.7 SI), cAMP-potentiated insulin secretion (G
123 16.7 + IBMX 100 AUC), cAMP-potentiated SI (G 16.7 + IBMX 100 SI), response to low glucose
124 plus adrenaline (G 1.7 + Ad 1 AUC), low glucose plus adrenaline inhibition index (II; G 1.7 + Ad
125 1 II), KCl-mediated insulin secretion (KCl 20 AUC), and KCl stimulation index (KCl 20 SI). We
126 also derived the following secretory traits from each glucagon trace: basal secretion, glucose-
127 inhibited glucagon secretion (G 16.7 AUC), glucose inhibition index (G 16.7 II), cAMP-
128 potentiated glucagon secretion (G 16.7 + IBMX 100), cAMP-potentiated SI (G 16.7 + IBMX 100
129 SI), low glucose plus adrenaline-induced secretion (G 1.7 + Ad 1 AUC), low glucose plus
130 adrenaline SI (G 1.7 + Ad 1 SI), KCl-mediated secretion (KCl 20 AUC), and the KCl stimulation
131 index (KCl 20 SI). These data highlight the marked heterogeneity in responses, with the
132 distribution of values shown for the total dataset and separately by sex and reported race and
133 ethnicity or primary predicted ancestry in **Extended Data Tables 1-4**. Spearman correlation

analyses revealed a significant correlation between donor age, sex, HbA1c, and BMI with multiple secretory traits (**Extended Data Figure 3**). Basal insulin secretion was positively correlated with HbA1c ($r = 0.14$, $p_{unadj} = 0.02$) and BMI ($r = 0.14$, $p_{unadj} = 0.02$). Age was negatively correlated with cAMP-potentiated insulin secretion ($r = -0.15$, $p_{unadj} = 0.01$) and the glucose stimulation index ($r = -0.12$, $p_{unadj} = 0.047$). The glucose stimulation index also was negatively correlated with sex ($r = -0.12$, $p_{unadj} = 0.04$), BMI ($r = -0.14$, $p_{unadj} =0.02$), and HbA1c ($r = -0.14$, $p_{unadj} = 0.02$). Additionally, HbA1c was positively correlated with cAMP-potentiated ($r = 0.16$, $p_{unadj} = 0.005$) and KCl-mediated glucagon secretion ($r = 0.12$, $p_{unadj} = 0.04$).

In multivariable models adjusting for donor age, sex, BMI, HbA1c, reported race or ethnicity, and islet isolation center, both pre-shipment culture time and islet transit time were significantly associated with multiple insulin and glucagon secretion traits (**Extended Data Figure 4A-B**). Given this, we added pre-shipment culture time and islet transit time into future multivariable regression models as additional covariates unless otherwise stated (8 covariates total). Of note, islet purity was associated with 3 islet functional traits; however, these data were unavailable for all observations for inclusion as a covariate in the regression model.

To remove potential confounding effects of other demographic and processing variables, we next explored associations between donor traits and secretory traits in multivariable analyses controlling for the other seven covariates. In these analyses, donor BMI was significantly associated with glucagon secretory traits (**Extended Data Figure 4D**). Specifically, BMI was negatively associated with basal (regression coefficient, $b = -0.20$, $p = 0.005$) and KCl-mediated depolarization of glucagon secretion ($b = -0.17$, $p = 0.03$) and positively associated with glucose-mediated glucagon inhibition ($b = 0.15$, $p = 0.03$; **Extended Data Figure 4D**). Donor age, sex, and reported race or ethnicity were associated with multiple secretory traits prior to, but not after adjusting for multiple comparisons (**Figure 3-4, Extended Data Figure 4E-F**). Interestingly, we found no differences in insulin or glucagon secretion between donors with HbA1c < 5.7% (n = 223) and those with HbA1c ≥ 5.7% (n = 76) (**Extended Data Figure 4C-D**).

For the human islet preparations for which genotyping data were available, we explored relationships between predicted genetic ancestry and islet function. We found that the relationships between primary predicted genetic ancestry and secretion were similar to those observed between reported race or ethnicity and insulin secretion. In addition, genetic ancestry had a statistically significant effect on basal insulin secretion (**Extended Data Figure 4E, Extended Data Figure 5A**).

Islet composition strongly influences hormone secretory response

Next, we explored associations between islet function, morphology (i.e., diameter, area, perimeter), composition, and hormone content (**Figure 5**). Interestingly, in both Spearman correlation and multivariable analyses, islet composition was highly associated with multiple secretion traits, especially insulin secretion (**Figure 5A-B, Extended Data Figure 3**). A higher percentage of β cells was associated with an increase in glucose-stimulated ($b = 0.23$, $p = 2.31 \times 10^{-4}$), cAMP-potentiated ($b = 0.35$, $p = 1.18 \times 10^{-8}$), and depolarization-mediated insulin secretion ($b = 0.30$, $p = 1.16 \times 10^{-6}$). These secretory traits were negatively associated with the percentage of islet α and δ cells. Additionally, the percentage of δ cells within the islets was negatively associated with the glucose stimulation index ($b = -0.13$, $p = 0.02$) and inhibition index of insulin secretion in response to low glucose and adrenaline ($b = -0.19$, $p = 1.76 \times 10^{-3}$). These associations were marked by relatively large effect sizes, as evidenced by the absolute value of the scaled regression coefficient (0.13 – 0.35).

Regarding the glucagon secretion traits, the percentage of α cells was positively associated with an increase in basal glucagon secretion ($b = 0.18$, $p = 3.42 \times 10^{-3}$) and total glucagon secreted in response to low glucose with adrenaline ($b = 0.21$, $p = 3.42 \times 10^{-3}$), while the percentage of β cells was negatively associated with these two traits (**Figure 5B**). Additionally, the percentage of α cells was negatively associated with the glucagon stimulation indices in response to both low glucose with adrenaline ($b = -0.17$, $p = 1.58 \times 10^{-2}$) and KCl ($b = -0.18$, $p = 9.28 \times 10^{-3}$), while the opposite was true for their association with the percentage of δ cells.

Alternative analyses adjusting for population structure using the first five principal components explaining genetic ancestry as covariates, where available, yielded similar results (**Extended Data Figure 6**). Although a few associations were lost in these analyses, partially due to the reduced sample size, these analyses also revealed associations between the percentage of islet δ cells and the cAMP-potentiated glucagon stimulation index ($b = 0.16$, $p = 2.05 \times 10^{-2}$) and the glucagon secreted in response to low glucose and epinephrine ($b = -0.20$, $p = 8.31 \times 10^{-3}$) in **Extended Data Figure 6B**.

As expected, β and α cell composition were strongly associated with insulin and glucagon content, respectively (**Figure 5C, Extended Data Figure 3, Extended Data Figure 6C**). However, associations between hormone content were more striking for glucagon secretion traits than insulin secretion traits after controlling for the eight covariates and adjusting for multiple comparisons (**Figure 5A-B**). Glucagon content was strongly associated with multiple glucagon secretion traits (**Figure 5B, Extended Data Figure 6B**), including basal glucagon secretion ($b = 0.40$, $p = 1.13 \times 10^{-13}$) and total glucagon secreted in response to all four

secretagogues; further, these associations were marked by relatively large effect sizes (0.21 – 0.42).

In contrast to the impact of islet composition and hormone content, we found no association between morphological traits (diameter, area, perimeter) of islets purified by hand-picking that underwent dynamic perifusion and any insulin or glucagon secretion traits (**Figure 5A-B**). Similar results were found when examining the relationship between the morphology-related traits of the islet preparation as a whole and islet functional traits (**Figure 5A-B**).

Islet composition is influenced by sex, reported race/ethnicity, and predicted genetic ancestry

Given the strong association between islet composition and hormone secretion, we analyzed relationships between islet composition and donor characteristics. On average, analyzed islets were composed of 58% β cells (range 25 – 92%), 34% α cells (range 3 – 68%), and 8% δ cells (range 1 – 19%). Similar to islet hormone secretion, there was significant donor-to-donor heterogeneity in islet endocrine cell composition (**Figure 6A**). Donor sex and reported race or ethnicity, and genetic ancestry had a global effect on the percentage of islet β and α cells in multivariable models incorporating the other seven covariates (**Figure 6B-D**). Specifically, female sex was associated with a higher percentage of α cells and a lower percentage of β cells (**Figure 6B**). We observed a statistically significant global effect of reported race or ethnicity on the percentage of β cells ($p = 0.003$) and α cells ($p = 0.003$). Additonally, individuals reported as Asian in comparison to White (**Figure 6C**), as well as those with predicted East Asian in comparison to European predicted ancestry (**Figure 6D**), had a higher percentage of β cells ($p = 0.0007$ and $p = 0.0001$, respectively) and a lower percentage of α cells ($p = 0.0007$ and $p = 0.0001$, respectively). There was a global effect of genetic ancestry on the percentage of β cells ($p = 0.0004$) and α cells ($p = 0.0004$) (**Extended Data Figure 7B**). We observed no significant effect of donor age, BMI, HbA1c, isolation center, pre-shipment culture time or islet transit time on islet composition in multivariable analyses (**Extended Data Figure 7A-B**).

We next investigated associations between islet hormone content, donor demographics, and islet processing traits (**Figure 6E-L, Extended Data Figure 7C-D**). We found a global effect of genetic ancestry on the insulin content ($p = 0.0451$). Additionally, individuals with predicted East Asian ancestry compared to those with European ancestry had higher insulin content ($p = 0.0048$) (**Figure 6H**). Insulin content was positively associated with donor age ($b = 0.14$, $p = 0.0496$) and negatively associated with transit time ($b = -0.15$, $p = 0.03$) in multivariable models controlling for the other seven covariates (**Extended Data Figure 7C-D**). Additionally, there was

234 a global effect of genetic ancestry on insulin content (p = 0.045, **Extended Data Figure 7D**). In
235 contrast, we found no associations between insulin content and donor sex, reported race or
236 ethnicity, BMI, HbA1c, or isolation center in similar multivariable analyses (**Figure 6F-G;**
237 **Extended Data Figure 7C-D**). Finally, female sex was associated with a higher glucagon
238 content (**Figure 6J)** and there was a global effect of sex on glucagon content (p = 0.015;
239 **Extended Data Figure 7D**), but no other associations were noted between glucagon content
240 and other demographic or processing traits in multivariable models (**Figure 6K-L; Extended**
241 **Data Figure 7C-D**). In analyses adjusting for population structure using the first five principal
242 components explaining genetic ancestry, female sex was also associated with a slight increase
243 in δ cell percentage (p = 0.049) (**Extended Data Figure 7E**), whereas there was no effect of
244 sex on glucagon content (**Extended Data Figure 7F**).

245 ***Genetic risk for diabetes is associated with islet composition***

246 Both T1D and T2D GWAS signals map to loci associated with islet-enriched genes and their
247 regulatory elements[6,37]. Furthermore, diabetes risk alleles have been associated with *in vivo*
248 measures of islet function in participants without diabetes and linked to worsened islet function
249 in those with T1D[38–40]. Thus, we were interested in determining how genetic risk for diabetes
250 influenced *in vitro* hormone secretion, content, and islet composition in our study. In the current
251 release of human islet preparations where donor genotyping data were available (n = 268), we
252 generated T1D and T2D GRS, utilizing 67 and 338 single-nucleotide variants, respectively,
253 based on previously published models[7,41]. Using these data, we investigated whether genetic
254 risk for diabetes predicted any observed differences in islet function, composition, or hormone
255 content in our dataset of human islet preparations from donors without diabetes. We further
256 investigated the role of "process-specific" partitioned genetic risk scores previously published
257 from clustering of intermediate traits to delineate heterogeneity in polygenic risk[42]. We
258 incorporated either the complete or partitioned GRS into multivariable models that included the
259 following as covariates with or without HbA1c: donor age, sex, BMI, HbA1c, isolation center,
260 pre-shipment culture time, islet transit time, and the first five principal components explaining
261 genetic ancestry (**Figure 7A-B; Extended Data Figure 8**). Interestingly, the T2D GRS was
262 positively associated with the percentage of islet δ cells with HbA1c covariate (b = 0.17, p =
263 0.019; **Figure 7B,** *top*) or without HbA1c covariate (b = 0.17, p = 0.016; **Figure 7B,** *bottom*). At
264 the same time, δ cells strongly influenced the islet hormone secretory traits (**Figure 5;**
265 **Extended Data Figure 6**), especially those of β cells, suggesting that HbA1c does not mediate
266 these associations. We detected no additional significant associations between T1D and T2D

267 GRS and either hormone secretion or content when including HbA1c covariate in our analysis
268 (**Extended Data Figure 8A-B**). In contrast, excluding HbA1c as a covariate not only detected a
269 significant association between the T2D GRS and the percentage of islet δ cells (**Figure 7B***,*
270 *bottom*) but also revealed a significant positive association between the T2D GRS and glucagon
271 content (**Extended Data Figure 8D**). Individual data points for associations of % δ cells and
272 T2D GRS are shown in **Extended Data Figure 9A.**

273 To further establish whether the underlying transcripts at T2D GWAS signals captured
274 within the T2D GRS were enriched in δ cells, we analyzed 87,505 islet cells (1877 δ cells) from
275 44 donors without diabetes using single-cell RNA sequencing data from the Human Pancreas
276 Analysis Program (HPAP)[43–46] (**Figure 7C-G**). Since the precise effector transcript remains
277 unknown for many T2D GWAS signals, we used the proximal gene to evaluate the polygenic
278 contributions of the 338 GRS variants (**Figure 7E** and **Extended Data Figure 9B**). Our analysis
279 demonstrated that several T2D GRS candidate genes are strongly upregulated in δ cells
280 (**Figure 7F**, significant genes highlighted in blue). Furthermore, we showed that the T2D GRS is
281 highly enriched for genes that are strongly expressed in δ cells (**Figure 7G**, with significant
282 genes highlighted in blue, and **Extended Data Figure 9C**).

283 **DISCUSSION**

284 Islet physiology is disrupted in both T1D and T2D. The pathways and cell-cell
285 communications that underlie islet dysfunction in diabetes are poorly understood, yet they may
286 have important implications in treatment strategies employing both pharmacologic agents and
287 islet or β cell replacement therapy. Recent emphasis on precision medicine approaches coupled
288 with increased utilization of single-cell technologies has highlighted an important role for
289 heterogeneity in diabetes classification, treatment, and molecular phenotypes[47–51]. To
290 understand how biological variation in humans impacts islet function and diabetes risk, we
291 generated this research resource from islets distributed through the NIH-funded IIDP. These
292 islets underwent pre-shipment assessment at one of five islet isolation centers followed by
293 centralized phenotyping and genotyping through the HIPP and HIGI programs. A strength of our
294 study is the inclusion of islets from a diverse group of U.S. organ donors with over 40% of
295 donors having a reported race or ethnicity other than White, non-Hispanic or Latino/a. The IIDP-
296 HIPP-HIGI workflow has enabled investigation for associations between inherent donor
297 characteristics, islet composition, genetic risk scores for T1D and T2D, and multiple insulin and
298 glucagon secretory traits. Our data can be accessed through the IIDP RDR, where researchers
299 can view and interrogate the dataset used for this analysis and propose their own unique

300 questions related to human islet biology using the larger RDR dataset. Images presented in this
301 report are available on the open-access Pancreatlas™ platform[52], which supports interactive
302 exploration of full-resolution islet imaging data.

303 Our phenotyping workflow includes an assessment of islet purity and viability, insulin and
304 glucagon secretion measured in a dynamic perifusion system, and a quantitative assessment of
305 islet composition in a sample of islets distinct from the islet aliquot used for perifusion. Studies
306 of the human pancreas suggest a greater than four-fold variation in β cell mass amongst
307 individuals without diabetes[53]. Not surprisingly, we observed a wide range of β cell secretory
308 responses to glucose, IBMX, and KCl, in line with previous reports [54–56]. While clinical studies
309 suggest that glucose tolerance declines with age, whether β cell function declines with age
310 independently of changes in insulin resistance and weight in individuals who maintain normal
311 glucose tolerance is not clear[57,58]. Similarly, the impact of donor age on insulin secretion *in vitro*
312 has been mixed in previous reports, with studies finding either no effect or a negative impact of
313 age on glucose-stimulated insulin secretion[55,59–62]. In addition, many studies report an effect of
314 BMI on multiple insulin secretory traits, while others have found no correlation[54,55,61,63]. In the
315 current study, Spearman correlation analyses revealed a significant positive relationship
316 between BMI and basal insulin secretion and a negative relationship between either BMI or age
317 and the glucose stimulation index. However, we detected no significant association between any
318 donor trait and insulin secretion in multivariable regression models adjusting for 7 other donor
319 and islet processing-related covariates. Our studies differ from these previous studies in that we
320 included a larger sample size of donors and controlled for multiple potentially confounding
321 demographic and islet processing features, which we and others have shown to impact *in vitro*
322 secretory responses[55,61,64].

323 In contrast to the weak effects of donor demographics on insulin secretion, islet
324 composition exhibited strong and consistent associations with insulin secretory traits in both
325 Spearman correlation and multivariable analyses. Consistent with observed heterogeneity in
326 hormone secretory responses, islet composition was highly heterogeneous amongst islet
327 preparations, with an approximately 4, 22, and 19-fold variation in the percentages of β, α, and
328 δ cells, respectively. β cell composition or a higher percentage of β cells was associated with
329 increased glucose-stimulated, cAMP-potentiated, and depolarization-mediated insulin secretion.
330 While islet isolation severs vascular and neuronal connections, the autonomy of the islet as a
331 mini-organ is well preserved after isolation, as demonstrated by the persistence of paracrine
332 interactions and electrical coupling that modulate islet cell-cell communication within islets[65].

333 Strikingly, although δ cells comprised a relatively low percentage of islet endocrine cell
334 composition, a higher percentage of δ cells negatively impacted most insulin secretion traits.
335 This finding is notable given a recent report showing that δ cells regulate the glycemic set point
336 in healthy mice and that ablation of the δ cell population leads to blood glucose lowering and
337 increased insulin secretion[66]. In multivariate analysis, we queried factors associated with T1D
338 and T2D GRS, identifying a positive association between the percentage of islet δ cells and the
339 T2D GRS. Of the 303 candidate genes that map to the 338 variants reflected in the T2D GRS,
340 181 of 303 (60%) genes were expressed (mean of normalized counts > 0.01) in δ cells. Notable
341 genes identified in this analysis include the transcription factor *HHEX*, which has previously
342 been shown to play an essential role in δ cell differentiation, with loss of *HHEX* leading to a
343 reduced number of δ cells, reduced islet somatostatin secretion, and increased insulin
344 secretion[67]. We identified δ cell expression of other notable genes with resolved effector
345 transcript status, including *DGKB*[4] and *GLP1R*[68,69], which have been associated with glycemia
346 and insulin secretory phenotypes in human studies.
347 Multiple glucagon secretory traits were associated with islet composition; however, we
348 found even stronger associations between glucagon content and total glucagon secreted in
349 response to all secretagogues used in this study. Interestingly, this same relationship was not
350 observed between insulin content and insulin secretory responses. One study comparing
351 murine β and α cells noted faster rates of glucagon granule exocytosis, larger readily releasable
352 pools, and a higher rate of refilling of these pools after depletion in α cells[70]. Therefore, it is
353 possible that these same mechanisms are at play in human islets and could explain differences
354 in the association between hormone content and secretion between β and α cells.
355 Our observations on the impact of islet composition on secretory traits raise an important
356 question of whether differences in cell composition are influenced by donor demographics
357 and/or genetics. Interestingly, we found a global effect of sex and reported race or ethnicity on
358 the percentage of islet β and α cells. Here, female donors had a higher percentage of α cells,
359 and donors reported as Asian exhibited a higher percentage of β cells. We note the relatively
360 small number of donors reported as Asian in the dataset, highlighting a need to confirm this
361 observation with larger sample sizes. Remarkably, a high T2D GRS was positively associated
362 with the percentage of islet δ cells, which was consistent with the finding that δ cell composition
363 negatively impacted most insulin secretion traits, highlighting the inhibitory potential of δ cell-
364 secreted factors, including somatostatin. Together, these data suggest that, in some individuals,
365 a genetic predisposition to having more δ cells may impact insulin secretory capacity and
366 glycemic setpoints, making one more susceptible to the development of T2D. This is further

supported by the structural basis for δ cell paracrine regulation in pancreatic islets[71]. However, the mechanisms by which genetic variation associated with altered T2D risk influences δ cell composition are unknown. Recent studies have utilized the abundance of known endocrine marker proteins to infer associations with gene and protein expression[56,64]; however, this is the first time to our knowledge that direct quantitative assessment of islet composition has been compared to hormone secretion.

In summary, this study has identified important relationships between donor demographics, genetics, islet processing, islet composition, hormone content, function, using human islet preparations from donors without diabetes. Given their impact on human islet function, these factors should be considered in interpreting future human islet studies. Further, they may have implications in strategies for β cell replacement therapy[72–74]. For example, in 2022 the FDA approved Lantidra[75], the first allogeneic pancreatic islet cellular therapy made from deceased donor pancreatic cells for the treatment of T1D to ameliorate problematic hypoglycemia with glucocorticoid-free immunosuppression[76]. Release criteria for islet grafts have historically included measures of glucose-stimulated insulin secretion, which predicts metabolic outcomes of human islet transplantation[77]. Our data highlight the impact of cell-cell interactions on islet function and suggest that islet composition may provide valuable insight into graft function post-transplant. Similarly, we expect that integrating these findings from 299 donors without diabetes with datasets generated using the same phenotyping and genotyping pipelines for islets from individuals with T1D and T2D, such as those generated by the Human Pancreas Analysis Program (HPAP)[43,46] will inform our understanding of diabetes pathophysiology and lead to the design of new therapies and disease prevention.

There are limitations of our analysis that should be acknowledged. First, our analysis was performed on islets isolated from the pancreas of organ donors following brain or circulatory death. Because the pancreas cannot be safely biopsied in living individuals, the analysis of post-mortem tissue remains an important caveat for most human islet research. While we evaluated the impact of donor demographic features and technical features of the isolation, we did not evaluate the impact of the reported cause of death on islet function or viability. There is some data to suggest that islet secretory function varies by category of reported cause of death (i.e., trauma, cerebrovascular, or cardiovascular)[78]. However, autopsy studies indicate that clinical assessment of the cause of death is prone to error in an estimated 13-38% of cases[79]. Further, whilst we examined factors impacting glucose-stimulated islet responses in detail, we did not investigate responses to other nutrients, such as fatty acids or amino acids, which also display significant donor-to-donor heterogeneity, as highlighted by a

401 recent report from Kolic et al.[56]. Finally, while this study is currently the largest of its type, we
402 had multiple observations that were nominally significant, supporting the need for larger studies
403 and expanded sample sizes. The diverse IIDP-HIPP-HIGI datasets represent a valuable and
404 continuously growing resource for the islet biology community, which can be used to generate
405 new scientific hypotheses and guide mechanistic studies of human islets. Future studies should
406 leverage this rich dataset to link islet secretory characteristics and composition with multi-omic
407 assessment and test these relationships in cohorts of donors, including controls and those with
408 pre-diabetes and diabetes, especially to understand cell-specific contributions to diabetes risk
409 and disease pathophysiology.

410 **RESOURCE AVAILABILITY**

411 ***Lead contact***

412 Further information and requests for resources and reagents should be directed to and will be
413 fulfilled by the lead contact, Marcela Brissova, PhD (marcela.brissova@vumc.org). Requests for
414 access to genetic data should be directed to Anna L. Gloyn, DPhil (agloyn@stanford.edu).

415 ***Materials availability***

416 This study did not generate new, unique reagents.

417 ***Data and code availability***

418 Data from the first release of 299 de-identified human islet preparations reported in this paper is
419 available in **Supplemental File 2.** The genetic risk scores and predicted ancestry for each
420 donor and the larger integrated dataset hosted are available for download from the IIDP
421 Research Data Repository. For more information on available datasets and how to access,
422 visit https://iidp.coh.org/Resources-Offered/Research-Data-Repository. Genotyping data were
423 deposited in the European Genome Phenome Archive (EGA) under accession number
424 EGAS50000000697 and are available through a data access agreement. All original code is
425 publicly available as of the date of publication. Code related to the generation of statistical
426 models is available at https://github.com/hakmook/HIPP_project. Code associated with the
427 prediction of genetic ancestry is available at https://github.com/gloynlab/GeneticAncestry. Any
428 additional information required to reanalyze the data reported in this paper is available from
429 either Dr. Brissova or Dr. Gloyn (genetic data) upon request.

430 **ACKNOWLEDGMENTS**

The authors would like to thank the organ donors and their families for their invaluable donations and acknowledge the IIDP collaborators who continue to make this work possible (**Supplemental File 1**). The authors would also like to thank Danielle Gibson (Vanderbilt University Medical Center) for her assistance with the HIPP studies, Dr. Emily Anderson-Baucum (Indiana University School of Medicine) for her helpful advice and edits, and Drs. Ha Vu, Stephen Parker, and Jie Liu for their critical reading of the manuscript and contributions to the edits. Research reported in this publication was supported by U42RR017673, UC4DK098085, U24DK098085, 1-RSC-2018-561-I-X, 1-RSC-2019-712-S-B, 1-RSC-2020-890-S-B, F30DK134041, T32GM007347, T32GM152284, R01DK129469, and The Leona M. and Harry B. Helmsley Charitable Trust. Whole-slide imaging was performed in the Islet and Pancreas Analysis Core of the Vanderbilt DRTC (DK20593).

We also acknowledge the resources provided by PanKbase (**https://www.pankbase.org**), which is supported by NIDDK U24DK138515 and U24DK138512, as well as supplemental funds from the NIH Office of Data Science Strategy (U01DK128847). This manuscript used data acquired from the database (**https://hpap.pmacs.upenn.edu/**) of the Human Pancreas Analysis Program (HPAP; RRID:SCR_016202). HPAP is part of a Human Islet Research Network (RRID:SCR_014393) consortium (UC4DK112217, U01DK123594, UC4DK112232, and U01DK123716).

AUTHOR CONTRIBUTIONS

Conceptualization: M.B., Y.D.P., H.K., D.C.S., S.A.S., A.L.G., J.C.N., and C.E.M.; Data curation: Y.D.P., D.C.S., S.A.S., H.S., A.L.H., A.B., K.X., and F.F.; Formal analysis: H.K., D.S., K.X., Y.D.P., S.A.S., H.S., and D.C.S.; Funding acquisition: C.E.M., K.A., A.L.G., J.C.N., and M.B.; Investigation: H.D., S.M., A.C., C.D., C.V.R., J.T., T.SR.B., R.A., G.P., A.E., R.J. V.S., and S.T.; Methodology: S.A.S., H.S., D.S., H.K., A.C.P., S.A.S. H.S. A.L.G and M.B.; Project administration: C.E.M., K.A., A.L.G., J.C.N., and M.B.; Software: JP.C.; Resources: M.B., C.E.M., A.L.G., J.C.N., JP.C., and A.C.P.; Supervision: M.B., C.E.M., A.L.G, J.C.N., H.K., A.C.P., and K.A.; Visualization: Y.D.P., S.A.S., H.S., and D.C.S.; Writing – original draft: Y.D.P., C.E.M., A.L.G., and M.B.; Writing – review & editing: all authors.

DECLARATION OF INTERESTS

A.L.G's spouse is an employee of Genentech and holds stock options in Roche.

461 **FIGURE LEGENDS**

462 **Figure 1. Integration of phenotyping and genotyping assessment of a diverse set of IIDP-**
463 **derived human islet preparations.** (**A**) Schematic illustrating the human islet phenotyping and
464 genotyping pipelines utilized by the HIPP and HIGI. The HIPP performs analysis of islet
465 morphology, purity, viability, histology, and function; the remaining sample is archived in a
466 biorepository for additional analyses. The HIGI receives a non-islet tissue sample and isolates
467 DNA to sequence for genetic ancestry prediction and calculation of genetic risk scores for type 1
468 and type 2 diabetes. (**B**) Descriptive statistics of donor demographics by sex and reported race
469 or ethnicity (n = 299). Values are reported as mean ± standard deviation, followed by the range.
470 (**C**) Descriptive statistics of donor demographics by sex and primary predicted ancestry (n =
471 268). Values are reported as mean ± standard deviation, followed by the range. **$p < 0.01$ vs.
472 male donors; ***$p < 0.001$ vs. male donors.

473 **Figure 2. Islet secretory function is highly heterogeneous amongst donors.** Average (**A**)
474 insulin and (**B**) glucagon secretion from donor islets normalized to islet equivalents (IEQs). Data
475 are displayed as mean ± 95% confidence interval (n = 299). (**C**) Schematic and tables
476 describing insulin and (**D**) glucagon secretion traits derived from individual islet secretion traces.
477 Descriptive statistics by sex and reported race/ethnicity are provided in **Extended Data Tables**
478 **1 and 2**. G – Glucose (mM); IBMX – isobutylmethylxanthine (μM); A – adrenaline (μM); KCl –
479 potassium chloride (mM).

480 **Figure 3. Islet secretion traits by sex.** Violin plots comparing (**A**) insulin and (**B**) glucagon
481 secretion traits between female (n = 115) and male (n = 184) donors. The solid line in each
482 violin plot depicts the median, and the dotted lines represent the 1st and 3rd quartiles. Global P-
483 value is based on the F-test while controlling for the seven covariates (age, sex, BMI, HbA1c,
484 islet isolation center, pre-shipment culture time, and islet transit time) and adjusting for multiple
485 comparisons. Comparisons where the unadjusted p-value (p_{unadj}) was significant are noted in
486 italics.

487 **Figure 4. Islet secretion traits by reported race or ethnicity.** Violin plots comparing (**A**)
488 insulin and (**B**) glucagon secretion traits by reported race or ethnicity (n = 12 Asian, n = 26 Black
489 or African American, n = 86 Hispanic or Latino/a, n = 175 White). The solid line in each violin
490 plot depicts the median, and the dotted lines represent the 1st and 3rd quartiles. Global p-value is
491 based on the F-test while controlling for the seven covariates (age, sex, BMI, HbA1c, islet
492 isolation center, pre-shipment culture time, and islet transit time) and adjusting for multiple

comparisons. Comparisons where the unadjusted p-value (p_{unadj}) was significant are noted in italics.

Figure 5. Islet composition and hormone content are associated with multiple islet secretory traits. (**A-B**) Heatmaps depicting regression coefficients of each morphologic variable for islets that underwent perifusion (n = 186), islet composition variable (n = 299), and total islet insulin and glucagon content (n = 299) after being incorporated into multivariable regression models controlling for age, sex, BMI, HbA1c, islet isolation center, reported race or ethnicity, pre-shipment culture time, and islet transit time for each (**A**) insulin or (**B**) glucagon secretion trait. (**C**) Heatmaps depicting regression coefficients of each islet composition variable after being incorporated into multivariable regression models for total insulin or glucagon content after adjusting for the eight covariates (n = 299). Adjusted p-values are indicated where *p < 0.05, **p < 0.01, and ***p < 0.001. Comparisons where the unadjusted p-value (p_{unadj}) was significant are noted in italics.

Figure 6. Islet composition and hormone content are highly variable and influenced by donor sex and ancestry. (**A**) Representative images of collagen gel-embedded islets and associated quantification of islet composition. Each point represents the average % β, % α, and % δ cells per donor (n = 299). Violin plots comparing islet composition by (**B**) donor sex, (**C**) reported race or ethnicity, and (**D**) predicted primary genetic ancestry. (**E**) Islet insulin content normalized to IEQ (n = 299). Violin plots comparing islet insulin content by (**F**) donor sex, (**G**) reported race or ethnicity, and (**H**) predicted primary genetic ancestry. (**F**) Islet glucagon content normalized to IEQ (n = 299). Violin plots comparing islet glucagon content by (**J**) donor sex, (**K**) reported race or ethnicity, and (**L**) predicted primary genetic ancestry. Donor sex: n = 115 female, n = 184 male. Reported race or ethnicity: n = 12 Asian, n = 26 Black or African American, n = 86 Hispanic or Latino/a, n = 175 White. Primary predicted genetic ancestry: n = 86 Admixed American, n = 21 African, n = 11 East Asian, n = 150 European. Adjusted global p-values are indicated where *p < 0.05, **p < 0.01, ***p < 0.001. For sex, reported race or ethnicity, and genetic ancestry, the global adjusted p-value is based on the F-test while controlling for the other seven covariates. INS – insulin; GCG – glucagon; SST – somatostatin.

Figure 7. Pancreatic islet δ cell composition is associated with a genetic risk score for type 2 diabetes derived from genome-wide association studies. (**A-B**) Heatmaps depicting coefficients of the GRS for (**A**) T1D and (**B**) T2D, along with partitioned GRS variables after being incorporated into multivariable regression models for each secretion trait, hormone content, and islet composition variable (n = 268). Each model included the following covariates:

526 donor age, sex, BMI, islet isolation center, pre-shipment culture time, islet transit time, and the
527 first five principal components explaining primary genetic ancestry, with the HbA1c covariate
528 (*top*) or without HbA1c covariate (*bottom*). “T1D GRS” encompasses the genetic risk for T1D
529 (67 total variants). “HLA DR/DQ” represents the sum of T1D risk at HLA-DR/DQ haplotypes.
530 “HLA Class 1” and “HLA Class 2” represent the sum of T1D risk at HLA class 1 and 2 alleles,
531 respectively, excluding HLA DR/DQ haplotypes. “Non-HLA” represents the sum of T1D risk from
532 variants outside the HLA region, genome-wide. “T2D GRS” encompasses genetic risk for T2D
533 (338 total variants). “Beta Cell,” “Proinsulin,” “Obesity,” “Lipodystrophy,” and “Liver/Lipid”
534 represent partitioned T2D GRS clusters encoding the related variants. Adjusted p-values are
535 indicated where $*p < 0.05$. Comparisons where the unadjusted p-value (p_{unadj}) was significant
536 are noted in italics. (**C**) Clustering of the HPAP single-cell RNA-seq data from 44 HPAP donors
537 without diabetes. (**D**) The number of cells of each type included in the analysis, including 1877 δ
538 cells. (**E**) The number of genes that were differentially expressed, with three different thresholds
539 for expression, in δ cells. (**F**) A dot plot showing T2D GRS genes that are differentially
540 expressed in δ cells (significant genes are shown in blue). (**G**) A heat map illustrating T2D GRS
541 genes that are differentially expressed in δ cells (significant genes are shown in blue).

EXTENDED DATA FIGURE AND TABLE LEGENDS

Extended Data Figure 1, related to Figure 1. Schematic of multimodal data integration by phenotyping and genotyping pipelines within Integrated Islet Distribution Program (IIDP) and data deposition in Resource Data Repository (RDR).

Extended Data Figure 2, related to Figure 1. Example HIPP procedures. (**A**) Representative images of a human islet preparation stained with dithizone (DTZ) to delineate islet versus non-islet tissue. Using the Count and Measure function in cellSens, images of DTZ-stained islets were utilized to quantify the total islet equivalents (IEQs), purity, and islet morphology. Tissue depicted in red on the image mark-up indicates positively identified islet tissue, while green marks non-islet tissue. (**B**) Representative images of handpicked islets pre- and post-perifusion. The red color on the image markup indicated positively identified islet tissue by the Count and Measure function in cellSens. The scale bar is 500 μm.

Extended Data Table 1, related to Figure 2. Insulin secretion is highly heterogeneous amongst donors. Descriptive statistics of the eleven insulin secretion traits by donor sex and reported race or ethnicity. Data are displayed as mean ± SD, followed by the range.

Extended Data Table 2, related to Figure 2. Glucagon secretion is highly heterogeneous amongst donors. Descriptive statistics of the nine glucagon secretion traits by donor sex and reported race or ethnicity. Data are displayed as mean ± SD, followed by the range.

Extended Data Table 3, related to Figure 2. Distribution of insulin secretion traits is similar in n = 268 subset. Descriptive statistics of the eleven insulin secretion traits by donor sex and genetic ancestry. Data are displayed as mean ± SD, followed by the range.

Extended Data Table 4, related to Figure 2. Distribution of glucagon secretion traits is similar in n = 268 subset. Descriptive statistics of the nine glucagon secretion traits by donor sex and genetic ancestry. Data are displayed as mean ± SD, followed by the range.

Extended Data Figure 3, related to Figure 2. Relationship between donor demographics, islet processing, islet morphology, and functional traits. Heatmap of Spearman r correlation coefficients between the indicated variables in the corresponding labeled row and column. For donor sex, the male was coded as 0 and female as 1. *$p < 0.05$; †$p < 0.01$; ‡$p < 0.001$. All p-values are unadjusted.

Extended Data Figure 4, related to Figures 3 and 4. Donor and islet processing traits correlate with islet function. (**A-B**) Heatmaps depicting regression coefficients of each islet

processing trait after being incorporated into multivariable regression models for each (**A**) insulin and (**B**) glucagon secretion trait. Each model included the following covariates: age, sex, reported race or ethnicity, BMI, HbA1c, and islet isolation center. Pre-shipment culture time and islet transit time were included as additional covariates for all subsequent models, unless noted otherwise. (**C-D**) Heatmaps depicting regression coefficients of donor age, BMI, and prediabetes status after being incorporated into multivariable regression models for each (**C**) insulin and (**D**) glucagon secretion trait while controlling for the other seven final covariates. Adjusted p-values are indicated where *p < 0.05, **p < 0.01, and **p < 0.001. For associations that are significant prior to adjusting to multiple comparisons, the unadjusted p-value is noted in italics. (**E-F**) Tables summarizing the global adjusted P-value when comparing differences by donor sex, reported race or ethnicity, genetic ancestry, and isolation center for each (**E**) insulin and (**F**) glucagon secretion trait. The global adjusted p-value is based on the F-test while controlling for the other seven covariates. Analyses involving genetic ancestry controlled for all covariates except reported race or ethnicity. n.s. indicates an insignificant global adjusted p-value and unadjusted p-value. For results that were significant prior to adjusting to multiple comparisons, the unadjusted p-value is noted in italics. n = 299 for all analyses except those involving islet purity (n = 269), elevated HbA1c (n = 76 elevated HbA1c, n = 223 normal HbA1c), and genetic ancestry (n = 268).

Extended Data Figure 5, related to Figure 4. Islet secretion traits by genetic ancestry. Violin plots comparing (**A**) insulin and (**B**) glucagon secretion traits by primary predicted genetic ancestry (n = 86 Admixed American, n = 21 African, n = 11 East Asian, n =150 European). The solid line in each violin plot depicts the median, and the dotted lines represent the 1st and 3rd quartiles. *p < 0.05 after adjusting for multiple comparisons. Comparisons where the unadjusted p-value (p_{unadj}) was significant are noted in italics. Global p-value is based on the F-test while controlling for the seven covariates (donor age, sex, BMI, HbA1c, islet isolation center, pre-shipment culture time, and islet transit time).

Extended Data Figure 6, Related to Figure 5. Islet composition and hormone content are associated with multiple islet secretory traits after adjusting for population structure using the first five principal components explaining genetic ancestry. (**A-B**) Heatmaps depicting regression coefficients of each morphologic variable for islets that underwent perifusion (n = 186), islet composition variable (n = 268), and total islet insulin and glucagon content (n = 268) after being incorporated into multivariable regression models controlling for age, sex, BMI, HbA1C, islet isolation center, islet transit time, pre-shipment culture time and the

606 first 5 principial components explaining genetic ancestry for each (**A**) insulin or (**B**) glucagon
607 secretion trait. (**C**) Heatmaps depicting regression coefficients of each islet composition variable
608 after being incorporated into multivariable regression models for total insulin or glucagon
609 content after adjusting for the eight covariates (n = 268). Adjusted p-values are indicated where
610 *p < 0.05, **p < 0.01, and ***p < 0.001. Comparisons where the unadjusted p-value (p_{unadj}) was
611 significant are noted in italics.

612 **Extended Data Figure 7, related to Figure 6. Correlation between donor demographics**
613 **and islet processing variables with islet composition and hormone content.** (**A**) Heatmaps
614 depicting regression coefficients of donor and islet processing variables when incorporated into
615 multivariable regression models with an islet composition variable (% β, α, or δ cells) as the
616 outcome variable. For models related to islet processing traits, the following covariates were
617 included: donor age, sex, reported race or ethnicity, BMI, HbA1c, and islet isolation center. For
618 donor traits, pre-shipment culture time and islet transit time were also included as covariates.
619 For associations that are significant before adjusting for multiple comparisons, the unadjusted p-
620 value is noted in italics. (**B**) Table summarizing the global adjusted p-value when comparing
621 differences by isolation center for each composition variable. The global adjusted p-value is
622 based on the F-test while controlling for the other seven covariates listed in **A**. (**C**) Heatmaps
623 depicting regression coefficients of donor and islet processing variables when incorporating into
624 multivariable regression models, insulin and glucagon content. For models related to islet
625 processing traits, the following covariates were included: age, sex, reported race or ethnicity,
626 BMI, HbA1c, and islet isolation center. For donor traits, pre-shipment culture time and islet
627 transit time were also included as covariates. Adjusted p-values are indicated where *p < 0.05.
628 (**D**) Table summarizing the global adjusted p-value when comparing differences by isolation
629 center for hormone content. The global adjusted p-value is based on the F-test while controlling
630 for the other seven covariates listed in **C**. (**E-F**) Violin plots comparing islet composition (**E**) and
631 glucagon content (**F**) by donor sex when adjusted for population structure, including seven
632 covariates: age, sex, BMI, HbA1c, islet isolation center, islet transit time, pre-shipment culture
633 time, plus 1st five principal components explaining genetic ancestry. Global adjusted p-values
634 based on the F-test while controlling for the other twelve covariates are indicated where *p <
635 0.05. For analyses including genetic ancestry as a covariate, n = 268; otherwise, n = 299 for all
636 other analyses.

637 **Extended Data Figure 8, related to Figure 7. Associations between T1D and T2D GRSs**
638 **and islet function and hormone content, including and disregarding HbA1c.** (**A-B**)

639 Heatmaps depicting coefficients of the GRS for (**A**) T1D and (**B**) T2D along with partitioned GRS
640 variables after being incorporated into multivariable regression models for each secretion,
641 hormone content, and islet composition variable (n = 268). Each model included the following
642 covariates: donor age, sex, BMI, islet isolation center, pre-shipment culture time, islet transit
643 time, and the first five principal components explaining primary genetic ancestry. Adjusted p-
644 values are indicated where *p < 0.05. For associations that are significant before changing to
645 multiple comparisons, the unadjusted p-value is noted in italics.

646 **Extended Data Figure 9, related to Figure 7. Mapping predicted T2D GWAS effector**
647 **transcripts in islet δ cells.** (**A**) Visualization of % δ cell composition in islets vs. T2D GRS. The
648 data were used for associations of % δ cells and T2D GRS after adjusting for the following
649 covariates: donor age, sex, BMI, islet isolation center, pre-shipment culture time, islet transit
650 time, and the first five principal components explaining primary genetic ancestry, with or without
651 HbA1c. (**B**) Number of signals included in the T2D GRS that map to an individual gene. Some
652 genes have more than one signal; therefore, 338 variants were mapped to 303 genes. (**C**)
653 Enrichment of T2D GRS for genes strongly expressed in δ cells.

654 **METHODS**

655 **EXPERIMENTAL MODEL AND STUDY PARTICIPANT DETAILS**

656 ***Primary human islet isolation***
657 Human islet preparations from cadaveric organ donors (n = 299) were isolated from five
658 affiliated islet isolation centers across the U.S and distributed to the Human Islet Phenotyping
659 Program through the IIDP from 2016-2024. Donor demographic information is detailed in **Figure**
660 **1**. De-identified human pancreatic specimens do not qualify as human subjects research under
661 the Vanderbilt or the Stanford Institutional Review Boards. All assays were performed on the
662 day of islet arrival. Islet preparations included in this manuscript (n = 299) were isolated from
663 five IIDP-affiliated isolation centers: Scharp-Lacy (n = 113), Southern California Islet Cell
664 Resource Center (n = 94), University of Miami (n = 30), University of Pennsylvania Islet
665 Transplant Center (n = 27), and the University of Wisconsin Human Islet Core (n = 35).

666 **METHOD DETAILS**

667 All human islet preparations were assessed according to standardized protocols established by
668 the HIPP and HIGI of the IIDP and are publicly available at https://iidp.coh.org/SOPs. All HIPP-

669 related assessments are conducted on the day of arrival. Methods are briefly summarized
670 below.

671 ***Islet purity and morphology***

672 A representative sample of the unpicked human islet preparation was prepared by combining a
673 320 µL aliquot of islet preparation and 680 µL CMRL medium. The representative sample was
674 stained with 50 µL of 1 mg/mL dithizone/DMSO/PBS (DTZ; Sigma, catalog #D5130) for 1-2 min
675 at room temperature. After adding 1 mL of CMRL medium, brightfield and darkfield images of
676 stained islets were captured at 10X magnification. Islet (stained) and non-islet (unstained) area
677 was determined using the Count and Measure function in cellSens (Olympus). Islet purity was
678 calculated as the following:

679 $$Islet\ Purity\ (\%) = \frac{Total\ islet\ tissue\ area}{Total\ islet\ tissue\ area + Total\ non-islet\ tissue\ area} \times 100$$

680 Using the Count and Measure function in cellSens, morphological characteristics of each
681 islet were also determined, including average islet radius, diameter, perimeter, and area.
682 Measurements were performed in triplicate to ensure accuracy.

683 ***Islet viability***

684 Qualitative assessment of islet viability upon arrival to the HIPP was performed using
685 fluorescein diacetate (FDA) and propidium iodide (PI). In brief, 400 µL of well-mixed total islet
686 suspension was added to a cell culture dish, and 10 µL of PI (Sigma Aldrich, catalog # P4170)
687 and 10 µL of FDA (Sigma Aldrich, catalog # F-7378) were added to the islet suspension in
688 succession. The plate was incubated in the dark for 15 mins, and the preparation was imaged
689 immediately using an Olympus SZX12 stereomicroscope system. Multiple fields of view were
690 captured from two replicates per donor to ensure that FDA/PI staining was visualized in 50-100
691 islets per preparation.

692 Additionally, a quantitative assessment of islet viability upon arrival to the HIPP was
693 performed using trypan blue dye. Two aliquots of ~100 handpicked islets were prepared in 1.5
694 mL tubes and washed three times using 2 mM EDTA/PBS via centrifugation at 200 rcf for 1 min
695 at 4 °C. Islets were dispersed into a single cell suspension using Accutase (Innovative Cell
696 Technologies, Inc, catalog # AT-104) and triturated at a slow speed for 10 minutes using an
697 electronic multichannel pipet with tips. The reaction was quenched with CMRL-1066 media
698 containing 10% FBS, 2 mM L-glutamine, and 1% penicillin/streptomycin, and cells were washed
699 twice via centrifugation at 500 rcf for 3 mins at 4 °C. The cell pellet was resuspended in 50-75
700 µL of CMRL-1066 medium by gently flicking the tube. Next, 10 µL of the cell suspension was

701 transferred to a new 1.5 mL tube and mixed with 10 µL Trypan Blue dye (Invitrogen, catalog #
702 T10282). The cell chamber slide was loaded with 10 µL of the mixture in each compartment,
703 and cell counts were acquired using the Countess II cell counter following instrument guidelines.
704 Cell counts were repeated for the second aliquot of handpicked islets. Reported viability
705 represents the average percentage of viable cells for duplicates of purified islets based on two
706 cell counts per aliquot.

707 ***Islet function in a dynamic perifusion system***

708 Islet function was assessed via dynamic perifusion. On the day islets were received, half of the
709 islet shipment (1000-5000 islet equivalents (IEQs)) was plated in a 10-cm non-tissue culture
710 treated dish and cultured in CMRL-1066 plus 10% FBS media at 37 °C and 5% CO_2 for 2 hours
711 prior to perifusion. Under microscope guidance, 267-300 IEQs were handpicked, islet size and
712 count were recorded, and high-resolution brightfield and darkfield images were captured at 10x
713 magnification. All islets were then transferred to a clear Eppendorf tube for loading into the
714 perifusion chamber, fractions were collected at 1 mL/min, and secretagogues were changed at
715 predetermined fractions. The following secretagogues were used for these perifusion studies:
716 5.6 mM glucose (baseline media; G 5.6), 16.7 mM glucose (G 16.7), 16.7 mM glucose with 100
717 µM isobutylmethylxanthine (IBMX; G 16.7 + IBMX 100), 1.7 mM glucose with 1 µM adrenaline
718 (G 1.7 + Ad 1), and 5.6 mM glucose with 20 mM KCl (G 5.6 + KCl 20). All secretagogues were
719 prepared in a perifusion medium containing 3.2 g $NaHCO_3$, 0.58 g L-glutamine, 0.11 g sodium
720 pyruvate, 1.11 g HEPES, 1 bottle DMEM, 1 g RIA-grade BSA, and 70 mg ascorbate in 1 L ultra-
721 purified water. The perifusion medium was filtered and de-gassed prior to preparation of
722 secretagogues.

723 After retrieving islets from the perifusion chamber and placing them into a 60-mm non-
724 treated culture dish, the IEQ of the retrieved islets was determined and islets were centrifuged
725 for 3 min at 200 rcf at room temperature. Islet hormone extracts were prepared by incubating
726 the retrieved islet pellet in 200 µL of fresh acid ethanol (50 µL 5N HCl + 5.5 mL 95% ethanol) for
727 24 hours. Samples were then spun at 3000 rcf for 5 min, aliquoted to 2 mL screwcap tubes, and
728 stored at -80 °C until further processing.

729 Insulin concentration in perifusates and islet extracts was measured via ELISA (2020 –
730 present; Human Insulin ELISA Kit, Mercodia, catalog # 10-1113-10) or RIA (Human Insulin-
731 Specific RIA, Millipore catalog # HI-14K). In the same samples, glucagon was also measured
732 via ELISA or RIA (2021 – present: Quantikine Glucagon ELISA Kit, R&D Systems catalog #
733 DGCG0; 2020 – 2021: HTRF Glucagon Detection Kit, Cisbio catalog #62CGLPEH; prior to
734 2020: Glucagon RIA, Millipore catalog #GL-32K). For each assay, standards and quality

735 controls were measured in duplicates, and perifusate and islet extract samples were measured
736 in duplicates (RIA) or single point (ELISA). Secreted insulin and glucagon concentrations were
737 normalized to IEQs and expressed as ng/100 IEQs/min. Alternatively, secreted insulin and
738 glucagon concentrations were normalized to their respective total hormone content and
739 expressed as %content/min.

740 ***Islet composition***

741 To assess islet composition and acinar cell components, an aliquot of the human islet
742 preparation was immobilized in a collagen I gel, embedded, and sectioned for histologic
743 analysis. An aliquot containing approximately 500 IEQs of the human islet preparation was
744 transferred into a 1.5 mL tube and washed three times in 1X PBS via centrifugation at 200 *xg* for
745 3 min. After removing the supernatant, 150 µL of collagen I working solution (563 µL collagen I
746 stock, 167 µL ultrapurified H_2O, 200 µL 5X DMEM, 20 µL HEPES, and 50 µL $NaHCO_3$) was
747 added to the islet pellet and the mixture was transferred into a well in the center of a 96-well
748 plate. The plate was incubated at 37 °C for 1.5 hours to allow the gel to solidify, then fixed on ice
749 for 15 min, filling the well with cold 4% paraformaldehyde/PBS. After the brief fixation, the
750 paraformaldehyde solution was removed and, using a 28 G needle, the gel was loosened from
751 the sides of the well and transferred with a spatula into a 12-well plate containing cold 4%
752 paraformaldehyde/PBS. The gel was fixed for an additional 45 min, shaking on ice, before being
753 washed three times with 1X PBS for 20 min shaking on ice, transferring the gel to a new well
754 containing fresh 1X PBS for each wash. Following an overnight incubation in 30% sucrose/1X
755 PBS, the collagen I gel was embedded into cryomolds containing OCT, imaged, and flash frozen
756 on dry ice. Islet gels were stored at -80 °C until sectioning.

757 Following sectioning of collagen gels, immunofluorescence staining of islets was
758 performed. In brief, 8-µm islet cryosections were allowed to thaw at room temperature and air-
759 dried for 30 mins. Sections were washed with 1X PBS 3 times for 5 mins to remove the OCT,
760 permeabilized with 0.2% Triton for 15 mins at room temperature, and washed 3 times in 1X
761 PBS. Sections were blocked with 5% normal donkey serum in 1X PBS at room temperature for
762 90 mins in a humidified chamber, then incubated overnight at 4 °C in a humidified chamber with
763 primary antibodies diluted in 0.1% Triton-X-100/1% BSA/1X PBS. Primary antibodies included:
764 C-peptide (rat, Developmental Studies Hybridoma Bank, GN-ID4, RRID:AB_2631151, 1:100),
765 Glucagon (mouse, Abcam, ab10988, RRID:AB_297642, 1:250), Glucagon (rabbit, Cell Signaling
766 Technology, 2760S, RRID:AB_659831, 1:100), Somatostatin (goat, Santa Cruz Biotechnology,
767 sc-7819, RRID:AB_2302603, 1:500), and HPX1 (mouse, Novus Biologicals, NBP1-18951,
768 RRID:AB_1625456, 1:100). Sections were washed with 1X PBS 3 times for 10 mins each, then

769 incubated for 1.5 hours at room temperature in a humidified chamber with secondary antibodies
770 diluted in 0.1% Triton/1% BSA/1X PBS. Secondary antibodies were purchased from Jackson
771 ImmunoResearch: Rat IgG-Cy2 (donkey, 712-225-150, RRID:AB_2340673, 1:500), Rat IgG-
772 Cy5 (donkey, 712-175-150, RRID:AB_2340671, 1:200), Mouse IgG-Cy3 (donkey, 715-165-150,
773 RRID:AB_2340813, 1:500), Rabbit IgG-Cy5 (donkey, 711-175-152, RRID:AB_2340607, 1:200),
774 Goat IgG-Cy5 (donkey, 705-175-147, RRID:AB_2340415, 1:200), and Mouse IgG-Cy3 (donkey,
775 715-165-150, RRID:AB_2340813, 1:500). Sections were counterstained with 1:25,000
776 DAPI/PBS for 10 mins at room temperature, then washed 3 times for 15 mins each in 1X PBS.
777 Sections were mounted with SlowFade Gold mounting medium, and islet sections were imaged
778 using a high-resolution whole slide scanning system (ScanScope FL, Aperio/Leica) connected
779 to a web-based digital slide repository powered by eSlide Manager and housed in the Vanderbilt
780 University Medical Center Data Center. A quantitative assessment of islet cell composition and
781 endocrine/acinar cell compartments was performed using a tissue classifier algorithm (Halo™,
782 Indica Labs) to analyze 50-100 islets per labeling experiment. Images presented herein are
783 deposited in the publicly available Pancreatlas™ platform[52], which allows the exploration of full-
784 resolution islet imaging data in an interactive manner
785 (https://pancreatlas.org/datasets/853/explore).

786 ***Genetic analysis***

787 DNA on 246/299 donors included in this release was isolated from human islet donor acinar
788 tissue at Vanderbilt using the Wizard Genomic DNA Purification Kit (Promega, catalog # A1120).
789 Quantification and quality assessment was performed using the Genomic DNA ScreenTape
790 assay. DNA was normalized to 50 ng/µL prior to shipment to the HIGI for further analysis. For 30
791 samples no acinar tissue was available. For 9 of these, DNA was extracted from FPPE sections
792 at Stanford using the Zymo QuickDNA FFPE Extraction Kit. For the remaining 23 donors DNA
793 was isolated from acinar tissue at Stanford using the DNAExtraction (Qiagen
794 DNeasyBlood&TissueKit, catalog # 69504).

795 Prior to genotyping all DNA samples were re-quantified using both the Nanodrop and
796 Qubit platforms. Samples containing less than 500 ng total DNA were speed-vacuumed and
797 concentrated prior to genotyping. All samples were genotyped using the Illumina Infinium
798 Omni2.5Exome V1.5 array with ~2.6 million single nucleotide variant (SNV) sites measured.
799 Genotyping data underwent quality control by filtering of SNVs with excess missing genotypes
800 (>2%), filtering of SNVs that do not conform to Hardy-Weinberg equilibrium ($p<1x10^{-6}$), and
801 removal of samples with either excess missing genotypes (>3%) or discordant genetic vs
802 recorded sex. For donor samples with excess missing genotypes, 10 µm-thick formalin-fixed

803 paraffin-embedded pancreas tissue slides were requested from IIDP. DNA was extracted using
804 the Zymo QuickDNA FFPE Extraction Kit and quantified by Nanodrop and Qubit. Samples were
805 then restored using the Infinium HD FFPE Restore Protocol and then re-genotyped. Since FFPE
806 samples have considerable DNA degradation, if these samples did not pass restoration, thicker
807 20 um FFPE slides were shipped from IIDP and DNA was extracted and sent for restoration and
808 genotyping. For samples that had discordant sex, an XY PCR was performed on the original
809 sample and an additional donor sample from IIDP (10-µm thick formalin-fixed paraffin-
810 embedded pancreas tissue slides). Genotyping results from the 270 donors passing QC
811 coordinates were then aligned to the positive strand on genome build GRCh38 and the data
812 imputed against the TOPMed R3 reference panel. After quality control and imputation, 69.4
813 million high-quality SNVs (R2 > 0.3) and 269 samples were available for analysis. Genetic risk
814 scores (GRS) for T1D and T2D were generated from previously published models using 67 and
815 338 SNVs respectively[7,41]. T2D partitioned genetic risk scores (pGRS) were generated using 94
816 SNVs with predetermined weights from a previous soft-clustering[42]. Genetic ancestry was
817 determined using a random forest classifier trained on the first 20 principal components of the
818 1000 Genomes reference panel (https://github.com/gloynlab/GeneticAncestry).

819 ***Differentiational expression of predicted T2D effector transcripts in δ cells***
820 Re-processed scRNA-seq data for islets of organ donors without diabetes were downloaded
821 from PanKbase (https://pankbase-data-v1.s3.us-west-
822 2.amazonaws.com/analysis_resources/single_cell_objects/min.cells0.01pct_min.features5pct_r
823 mDoublets_harmony_data.Rds). The dataset included 87,505 islet cells (1877 δ cells) from 44
824 donors, https://zenodo.org/records/15588240, and is available for the lookup on Pancreatlas
825 https://pancreatlas.org/datasets/1138/explore/omics/17. Additional lookup data for δ gene
826 expression in human islets from donors without diabetes is available here
827 https://powersbrissovalab.shinyapps.io/scRNAseq-Islets/. The variants (N = 338) in the
828 calculation of the genetic risk score were mapped to the closest genes (N = 303) using
829 BEDTools with the gene annotation from Ensembl (v112). The number of expressed genes in
830 islets and δ cells was estimated by applying multiple thresholds, 0.001, 0.01, and 0.1, on the
831 mean normalized counts across all genes and δ cells only, respectively. Differential gene
832 expression analysis between the δ cells and the rest of the cells, and each of the other cell
833 types, on the closest genes was performed using the Wilcoxon rank-sum method in the scanpy
834 package (v1.10.4), with p values adjusted by the Benjamini-Hochberg method. Significant genes
835 (padj < 0.05) that are upregulated in δ cells (logfoldchanges > 0, higher expression in δ cells

836 than in other types of cells) and expressed in at least 20% of δ cells are visualized in dot plot
837 showing mean gene expression and fraction of cells, ordered by descending logfoldchanges,
838 and heatmap showing effect size (logfoldchanges), with the marker gene of δ cells (SST)
839 included for reference. The blue color in **Figure 7F-G** highlights genes with a fold change
840 greater than 2 when comparing δ cells with the remaining cells. A Fisher test was performed to
841 check if there is an enrichment of the closest genes in the differentially expressed genes
842 between δ cells and other cell types.

843 QUANTIFICATION AND STATISTICAL ANALYSIS

844 *Hormone secretion traits*

845 Using the insulin and glucagon secretion traces normalized to IEQ, eleven insulin secretion
846 traits and nine glucagon secretion traits were defined and calculated as illustrated in **Figure 2C-**
847 **D**.

848 *Statistical analysis*

849 To determine demographic, islet processing, and morphologic variables associated with
850 differences in islet secretory function, we first performed Spearman correlation analyses. For
851 variables with a statistically significant association with islet secretory traits, we utilized
852 multivariable regression models to examine the relationship among the explanatory variables
853 and the outcome variable of interest. For each model, we controlled for the following potential
854 confounders, unless otherwise noted: donor age, sex, BMI, isolation center, HbA1c, reported
855 race or ethnicity, pre-shipment culture time, and transit time. A statistically significant regression
856 coefficient for the explanatory variable (p-value < 0.05) denoted a significant association. Given
857 multiple p-values, we adjusted for the false discovery rate (FDR) at 0.05 to control for multiple
858 comparisons.

859 Similarly, to explore potential differences based on prediabetes status or sex, we used
860 multivariable regression models. In these models, an indicator variable (0 for normal, 1 for pre-
861 diabetes participants; 0 for male, 1 for female) acted as the explanatory variable. For
862 prediabetes-related associations, we controlled for all eight of the aforementioned potential
863 confounders except HbA1c. For sex-related associations, we controlled all potential
864 confounders except donor sex. The significance of the regression coefficient (b) for the group
865 indicator (p-value < 0.05) indicated a notable difference in the outcome variable between the
866 two groups.

To ensure comparability of regression coefficients across models, we normalized the outcome variables and all continuous explanatory variables, including covariates. This normalization involved centering the variables by subtracting their mean and scaling them by their standard deviation. However, this procedure was not applied to categorical covariates in the model, such as center, self-reported ancestry, and sex. Statistical analyses were all performed using R Statistical Software version 4.3.0 (R Foundation for Statistical Computing, Vienna, Austria) and GraphPad Prism version 10.

REFERENCES

1. Centers for Disease Control and Prevention National Diabetes Statistics Report. https://www.cdc.gov/diabetes/php/data-research/index.html.

2. Parker, E.D., Lin, J., Mahoney, T., Ume, N., Yang, G., Gabbay, R.A., ElSayed, N.A., and Bannuru, R.R. (2023). Economic Costs of Diabetes in the U.S. in 2022. Diabetes Care *47*, 26–43. https://doi.org/10.2337/dci23-0085.

3. Mattis, K.K., and Gloyn, A.L. (2020). From Genetic Association to Molecular Mechanisms for Islet-cell Dysfunction in Type 2 Diabetes. J. Mol. Biol. *432*, 1551–1578. https://doi.org/10.1016/j.jmb.2019.12.045.

4. Viñuela, A., Varshney, A., Bunt, M. van de, Prasad, R.B., Asplund, O., Bennett, A., Boehnke, M., Brown, A.A., Erdos, M.R., Fadista, J., et al. (2020). Genetic variant effects on gene expression in human pancreatic islets and their implications for T2D. Nat Commun *11*, 4912. https://doi.org/10.1038/s41467-020-18581-8.

5. Rich, S.S., Erlich, H., and Concannon, P. (2018). Genetics of Type 1 Diabetes. In Diabetes in America. 3rd edition. Bethesda (MD): National Institute of Diabetes and Digestive and Kidney Diseases (US), C. C. Cowie, S. S. Casagrande, A. Menke, M. A. Cissell, M. S. Eberhardt, J. B. Meigs, E. W. Gregg, W. C. Knowler, E. Barrett-Connor, D. J. Becker, et al., eds., p. Chapter 12.

6. Krentz, N.A.J., and Gloyn, A.L. (2020). Insights into pancreatic islet cell dysfunction from type 2 diabetes mellitus genetics. Nat. Rev. Endocrinol. *16*, 202–212. https://doi.org/10.1038/s41574-020-0325-0.

7. Mahajan, A., Spracklen, C.N., Zhang, W., Ng, M.C.Y., Petty, L.E., Kitajima, H., Yu, G.Z., Rüeger, S., Speidel, L., Kim, Y.J., et al. (2022). Multi-ancestry genetic study of type 2 diabetes highlights the power of diverse populations for discovery and translation. Nat. Genet. *54*, 560–572. https://doi.org/10.1038/s41588-022-01058-3.

8. Unger, R.H., Aguilar-Parada, E., Müller, W.A., and Eisentraut, A.M. (1970). Studies of pancreatic alpha cell function in normal and diabetic subjects. J Clin Invest *49*, 837–848. https://doi.org/10.1172/jci106297.

9. Gerich, J.E., Langlois, M., Noacco, C., Karam, J.H., and Forsham, P.H. (1973). Lack of Glucagon Response to Hypoglycemia in Diabetes: Evidence for an Intrinsic Pancreatic Alpha Cell Defect. Science *182*, 171–173. https://doi.org/10.1126/science.182.4108.171.

10. Sherr, J., Tsalikian, E., Fox, L., Buckingham, B., Weinzimer, S., Tamborlane, W.V., White, N.H., Arbelaez, A.M., Kollman, C., Ruedy, K.J., et al. (2014). Evolution of Abnormal Plasma Glucagon Responses to Mixed-Meal Feedings in Youth With Type 1 Diabetes During the First 2 Years After Diagnosis. Diabetes Care *37*, 1741–1744. https://doi.org/10.2337/dc13-2612.

11. Færch, K., Vistisen, D., Pacini, G., Torekov, S.S., Johansen, N.B., Witte, D.R., Jonsson, A., Pedersen, O., Hansen, T., Lauritzen, T., et al. (2016). Insulin Resistance Is Accompanied by Increased Fasting Glucagon and Delayed Glucagon Suppression in Individuals With Normal and Impaired Glucose Regulation. Diabetes *65*, 3473–3481. https://doi.org/10.2337/db16-0240.

12. Brissova, M., Haliyur, R., Saunders, D., Shrestha, S., Dai, C., Blodgett, D.M., Bottino, R., Campbell-Thompson, M., Aramandla, R., Poffenberger, G., et al. (2018). α Cell Function and Gene Expression Are Compromised in Type 1 Diabetes. Cell Reports *22*, 2667–2676. https://doi.org/10.1016/j.celrep.2018.02.032.

13. Camunas-Soler, J., Dai, X.-Q., Hang, Y., Bautista, A., Lyon, J., Suzuki, K., Kim, S.K., Quake, S.R., and MacDonald, P.E. (2020). Patch-Seq Links Single-Cell Transcriptomes to Human Islet Dysfunction in Diabetes. Cell Metab *31*, 1017-1031.e4. https://doi.org/10.1016/j.cmet.2020.04.005.

14. Omar-Hmeadi, M., Lund, P.-E., Gandasi, N.R., Tengholm, A., and Barg, S. (2020). Paracrine control of α-cell glucagon exocytosis is compromised in human type-2 diabetes. Nat Commun *11*, 1896. https://doi.org/10.1038/s41467-020-15717-8.

15. Kellard, J.A., Rorsman, N.J.G., Hill, T.G., Armour, S.L., Bunt, M. van de, Rorsman, P., Knudsen, J.G., and Briant, L.J.B. (2020). Reduced somatostatin signalling leads to hypersecretion of glucagon in mice fed a high-fat diet. Mol. Metab. *40*, 101021. https://doi.org/10.1016/j.molmet.2020.101021.

16. Vergari, E., Denwood, G., Salehi, A., Zhang, Q., Adam, J., Alrifaiy, A., Asterholm, I.W., Benrick, A., Chibalina, M.V., Eliasson, L., et al. (2020). Somatostatin secretion by Na+-dependent Ca2+-induced Ca2+ release in pancreatic delta cells. Nat. Metab. *2*, 32–40. https://doi.org/10.1038/s42255-019-0158-0.

17. Dai, X.-Q., Camunas-Soler, J., Briant, L.J.B., Santos, T. dos, Spigelman, A.F., Walker, E.M., Drigo, R.A. e, Bautista, A., Jones, R.C., Avrahami, D., et al. (2021). Heterogenous impairment of α cell function in type 2 diabetes is linked to cell maturation state. Cell Metab *34*, 256-268.e5. https://doi.org/10.1016/j.cmet.2021.12.021.

18. Hill, T.G., Gao, R., Benrick, A., Kothegala, L., Rorsman, N., Santos, C., Acreman, S., Briant, L.J., Dou, H., Gandasi, N.R., et al. (2024). Loss of electrical β-cell to δ-cell coupling underlies impaired hypoglycaemia-induced glucagon secretion in type-1 diabetes. Nat. Metab., 1–12. https://doi.org/10.1038/s42255-024-01139-z.

19. Brissova, M., Fowler, M.J., Nicholson, W.E., Chu, A., Hirshberg, B., Harlan, D.M., and Powers, A.C. (2005). Assessment of Human Pancreatic Islet Architecture and Composition by Laser Scanning Confocal Microscopy. J Histochem Cytochem *53*, 1087–1097. https://doi.org/10.1369/jhc.5c6684.2005.

20. Cabrera, O., Berman, D.M., Kenyon, N.S., Ricordi, C., Berggren, P.-O., and Caicedo, A. (2006). The unique cytoarchitecture of human pancreatic islets has implications for islet cell function. Proc National Acad Sci *103*, 2334–2339. https://doi.org/10.1073/pnas.0510790103.

21. Rodriguez-Diaz, R., Abdulreda, M.H., Formoso, A.L., Gans, I., Ricordi, C., Berggren, P.-O., and Caicedo, A. (2011). Innervation Patterns of Autonomic Axons in the Human Endocrine Pancreas. Cell Metab. *14*, 45–54. https://doi.org/10.1016/j.cmet.2011.05.008.

22. Dai, C., Brissova, M., Hang, Y., Thompson, C., Poffenberger, G., Shostak, A., Chen, Z., Stein, R., and Powers, A.C. (2012). Islet-enriched gene expression and glucose-induced insulin

951 secretion in human and mouse islets. Diabetologia *55*, 707–718.
952 https://doi.org/10.1007/s00125-011-2369-0.

953 23. Brissova, M., Shostak, A., Fligner, C.L., Revetta, F.L., Washington, M.K., Powers, A.C., and
954 Hull, R.L. (2015). Human Islets Have Fewer Blood Vessels than Mouse Islets and the Density of
955 Islet Vascular Structures Is Increased in Type 2 Diabetes. J. Histochem. Cytochem. *63*, 637–
956 645. https://doi.org/10.1369/0022155415573324.

957 24. Alcazar, O., and Buchwald, P. (2019). Concentration-Dependency and Time Profile of
958 Insulin Secretion: Dynamic Perifusion Studies With Human and Murine Islets. Front. Endocrinol.
959 *10*, 680. https://doi.org/10.3389/fendo.2019.00680.

960 25. Gloyn, A.L., Ibberson, M., Marchetti, P., Powers, A.C., Rorsman, P., Sander, M., and
961 Solimena, M. (2022). Every islet matters: improving the impact of human islet research. Nat.
962 Metab. *4*, 970–977. https://doi.org/10.1038/s42255-022-00607-8.

963 26. Kaddis, J.S., Olack, B.J., Sowinski, J., Cravens, J., Contreras, J.L., and Niland, J.C. (2009).
964 Human Pancreatic Islets and Diabetes Research. Jama *301*, 1580–1587.
965 https://doi.org/10.1001/jama.2009.482.

966 27. Qian, D., Kaddis, J., and Niland, J.C. (2007). A matching algorithm for the distribution of
967 human pancreatic islets. Comput. Stat. Data Anal. *51*, 5494–5506.
968 https://doi.org/10.1016/j.csda.2007.02.030.

969 28. Niland, J.C., Stiller, T., Cravens, J., Sowinski, J., Kaddis, J., and Qian, D. (2010).
970 Effectiveness of a Web-Based Automated Cell Distribution System. Cell Transplant. *19*, 1133–
971 1142. https://doi.org/10.3727/096368910x505486.

972 29. Brissova, M., Niland, J.C., Cravens, J., Olack, B., Sowinski, J., and Evans-Molina, C. (2019).
973 The Integrated Islet Distribution Program answers the call for improved human islet phenotyping
974 and reporting of human islet characteristics in research articles. Diabetologia *62*, 1312–1314.
975 https://doi.org/10.1007/s00125-019-4876-3.

976 30. Haliyur, R., Tong, X., Sanyoura, M., Shrestha, S., Lindner, J., Saunders, D.C., Aramandla,
977 R., Poffenberger, G., Redick, S.D., Bottino, R., et al. (2018). Human islets expressing HNF1A
978 variant have defective β cell transcriptional regulatory networks. J. Clin. Investig. *129*, 246–251.
979 https://doi.org/10.1172/jci121994.

980 31. Hart, N.J., Aramandla, R., Poffenberger, G., Fayolle, C., Thames, A.H., Bautista, A.,
981 Spigelman, A.F., Babon, J.A.B., DeNicola, M.E., Dadi, P.K., et al. (2018). Cystic fibrosis–related
982 diabetes is caused by islet loss and inflammation. JCI Insight *3*, e98240.
983 https://doi.org/10.1172/jci.insight.98240.

984 32. Shrestha, S., Saunders, D.C., Walker, J.T., Camunas-Soler, J., Dai, X.-Q., Haliyur, R.,
985 Aramandla, R., Poffenberger, G., Prasad, N., Bottino, R., et al. (2021). Combinatorial
986 transcription factor profiles predict mature and functional human islet α and β cells. Jci Insight *6*,
987 e151621. https://doi.org/10.1172/jci.insight.151621.

988 33. Haliyur, R., Walker, J.T., Sanyoura, M., Reihsmann, C.V., Shrestha, S., Aramandla, R.,
989 Poffenberger, G., Ramirez, A.H., Redick, S.D., Babon, J.A.B., et al. (2021). Integrated Analysis

990 of the Pancreas and Islets Reveals Unexpected Findings in Human Male With Type 1 Diabetes.
991 J Endocr Soc *5*, bvab162. https://doi.org/10.1210/jendso/bvab162.

992 34. Doliba, N.M., Rozo, A.V., Roman, J., Qin, W., Traum, D., Gao, L., Liu, J., Manduchi, E., Liu,
993 C., Golson, M.L., et al. (2022). α Cell dysfunction in islets from nondiabetic, glutamic acid
994 decarboxylase autoantibody–positive individuals. J. Clin. Investig. *132*, e156243.
995 https://doi.org/10.1172/jci156243.

996 35. Walker, J.T., Saunders, D.C., Rai, V., Chen, H.-H., Orchard, P., Dai, C., Pettway, Y.D.,
997 Hopkirk, A.L., Reihsmann, C.V., Tao, Y., et al. (2023). Genetic risk converges on regulatory
998 networks mediating early type 2 diabetes. Nature *624*, 621–629. https://doi.org/10.1038/s41586-
999 023-06693-2.

1000 36. Organ Procurement and Transplantation Network (OPTN) and Scientific Registry of
1001 Transplant Recipients (SRTR) (2024). OPTN/SRTR 2022 Annual Data Report. U.S. Department
1002 of Health and Human Services, Health Resources and Services Administration; 2024.

1003 37. Fløyel, T., Kaur, S., and Pociot, F. (2015). Genes Affecting β-Cell Function in Type 1
1004 Diabetes. Curr. Diabetes Rep. *15*, 97. https://doi.org/10.1007/s11892-015-0655-9.

1005 38. Dimas, A.S., Lagou, V., Barker, A., Knowles, J.W., Mägi, R., Hivert, M.-F., Benazzo, A.,
1006 Rybin, D., Jackson, A.U., Stringham, H.M., et al. (2014). Impact of Type 2 Diabetes
1007 Susceptibility Variants on Quantitative Glycemic Traits Reveals Mechanistic Heterogeneity.
1008 Diabetes *63*, 2158–2171. https://doi.org/10.2337/db13-0949.

1009 39. Brorsson, C.A., Nielsen, L.B., Andersen, M.L., Kaur, S., Bergholdt, R., Hansen, L.,
1010 Mortensen, H.B., Pociot, F., Størling, J., and Diabetes, H.S.G. on C. (2016). Genetic Risk Score
1011 Modelling for Disease Progression in New-Onset Type 1 Diabetes Patients: Increased Genetic
1012 Load of Islet-Expressed and Cytokine-Regulated Candidate Genes Predicts Poorer Glycemic
1013 Control. J. Diabetes Res. *2016*, 9570424. https://doi.org/10.1155/2016/9570424.

1014 40. Snethlage, C.M.F., Balvers, M., Ferwerda, B., Rampanelli, E., Groen, P. de, Roep, B.O.,
1015 Herrema, H., McDonald, T.J., Raalte, D.H. van, Weedon, M.N., et al. (2024). Associations
1016 between diabetes-related genetic risk scores and residual beta cell function in type 1 diabetes:
1017 the GUTDM1 study. Diabetologia, 1–12. https://doi.org/10.1007/s00125-024-06204-6.

1018 41. Sharp, S.A., Rich, S.S., Wood, A.R., Jones, S.E., Beaumont, R.N., Harrison, J.W.,
1019 Schneider, D.A., Locke, J.M., Tyrrell, J., Weedon, M.N., et al. (2019). Development and
1020 Standardization of an Improved Type 1 Diabetes Genetic Risk Score for Use in Newborn
1021 Screening and Incident Diagnosis. Diabetes Care *42*, 200–207. https://doi.org/10.2337/dc18-
1022 1785.

1023 42. DiCorpo, D., LeClair, J., Cole, J.B., Sarnowski, C., Ahmadizar, F., Bielak, L.F., Blokstra, A.,
1024 Bottinger, E.P., Chaker, L., Chen, Y.-D.I., et al. (2022). Type 2 Diabetes Partitioned Polygenic
1025 Scores Associate With Disease Outcomes in 454,193 Individuals Across 13 Cohorts. Diabetes
1026 Care *45*, 674–683. https://doi.org/10.2337/dc21-1395.

1027 43. Kaestner, K.H., Powers, A.C., Naji, A., Consortium, H., and Atkinson, M.A. (2019). NIH
1028 Initiative to Improve Understanding of the Pancreas, Islet, and Autoimmunity in Type 1

1029 Diabetes: The Human Pancreas Analysis Program (HPAP). Diabetes *68*, 1394–1402.
1030 https://doi.org/10.2337/db19-0058.

1031 44. Patil, A.R., Schug, J., Naji, A., Kaestner, K.H., Faryabi, R.B., and Vahedi, G. (2023). Single-
1032 cell expression profiling of islets generated by the Human Pancreas Analysis Program. Nat.
1033 Metab. *5*, 713–715. https://doi.org/10.1038/s42255-023-00806-x.

1034 45. Fasolino, M., Schwartz, G.W., Patil, A.R., Mongia, A., Golson, M.L., Wang, Y.J., Morgan, A.,
1035 Liu, C., Schug, J., Liu, J., et al. (2022). Single-cell multi-omics analysis of human pancreatic
1036 islets reveals novel cellular states in type 1 diabetes. Nat Metabolism *4*, 284–299.
1037 https://doi.org/10.1038/s42255-022-00531-x.

1038 46. Shapira, S.N., Naji, A., Atkinson, M.A., Powers, A.C., and Kaestner, K.H. (2022).
1039 Understanding islet dysfunction in type 2 diabetes through multidimensional pancreatic
1040 phenotyping: The Human Pancreas Analysis Program. Cell Metab. *34*, 1906–1913.
1041 https://doi.org/10.1016/j.cmet.2022.09.013.

1042 47. Tobias, D.K., Merino, J., Ahmad, A., Aiken, C., Benham, J.L., Bodhini, D., Clark, A.L.,
1043 Colclough, K., Corcoy, R., Cromer, S.J., et al. (2023). Second international consensus report on
1044 gaps and opportunities for the clinical translation of precision diabetes medicine. Nat. Med. *29*,
1045 2438–2457. https://doi.org/10.1038/s41591-023-02502-5.

1046 48. Dorrell, C., Schug, J., Canaday, P.S., Russ, H.A., Tarlow, B.D., Grompe, M.T., Horton, T.,
1047 Hebrok, M., Streeter, P.R., Kaestner, K.H., et al. (2016). Human islets contain four distinct
1048 subtypes of β cells. Nat. Commun. *7*, 11756. https://doi.org/10.1038/ncomms11756.

1049 49. Wigger, L., Barovic, M., Brunner, A.-D., Marzetta, F., Schöniger, E., Mehl, F., Kipke, N.,
1050 Friedland, D., Burdet, F., Kessler, C., et al. (2021). Multi-omics profiling of living human
1051 pancreatic islet donors reveals heterogeneous beta cell trajectories towards type 2 diabetes.
1052 Nat Metabolism *3*, 1017–1031. https://doi.org/10.1038/s42255-021-00420-9.

1053 50. Weng, C., Gu, A., Zhang, S., Lu, L., Ke, L., Gao, P., Liu, X., Wang, Y., Hu, P., Plummer, D.,
1054 et al. (2023). Single cell multiomic analysis reveals diabetes-associated β-cell heterogeneity
1055 driven by HNF1A. Nat. Commun. *14*, 5400. https://doi.org/10.1038/s41467-023-41228-3.

1056 51. Wang, G., Chiou, J., Zeng, C., Miller, M., Matta, I., Han, J.Y., Kadakia, N., Okino, M.-L.,
1057 Beebe, E., Mallick, M., et al. (2023). Integrating genetics with single-cell multiomic
1058 measurements across disease states identifies mechanisms of beta cell dysfunction in type 2
1059 diabetes. Nat. Genet. *55*, 984–994. https://doi.org/10.1038/s41588-023-01397-9.

1060 52. Saunders, D.C., Messmer, J., Kusmartseva, I., Beery, M.L., Yang, M., Atkinson, M.A.,
1061 Powers, A.C., Cartailler, J.-P., and Brissova, M. (2020). Pancreatlas: Applying an Adaptable
1062 Framework to Map the Human Pancreas in Health and Disease. Patterns *1*, 100120.
1063 https://doi.org/10.1016/j.patter.2020.100120.

1064 53. Meier, J.J., Butler, A.E., Saisho, Y., Monchamp, T., Galasso, R., Bhushan, A., Rizza, R.A.,
1065 and Butler, P.C. (2008). β-Cell Replication Is the Primary Mechanism Subserving the Postnatal
1066 Expansion of β-Cell Mass in Humans. Diabetes *57*, 1584–1594. https://doi.org/10.2337/db07-
1067 1369.

1068 54. Kayton, N.S., Poffenberger, G., Henske, J., Dai, C., Thompson, C., Aram, la, R., Shostak,
1069 A., Nicholson, W., Brissova, M., et al. (2015). Human islet preparations distributed for research
1070 exhibit a variety of insulin-secretory profiles. Am J Physiol Endocrinol Metab *308*, E592–E602.
1071 https://doi.org/10.1152/ajpendo.00437.2014.

1072 55. Henquin, J. (2018). Influence of organ donor attributes and preparation characteristics on
1073 the dynamics of insulin secretion in isolated human islets. Physiol. Rep. *6*, e13646.
1074 https://doi.org/10.14814/phy2.13646.

1075 56. Kolic, J., Sun, W.G., Cen, H.H., Ewald, J.D., Rogalski, J.C., Sasaki, S., Sun, H., Rajesh, V.,
1076 Xia, Y.H., Moravcova, R., et al. (2024). Proteomic predictors of individualized nutrient-specific
1077 insulin secretion in health and disease. Cell Metab. *36*, 1619-1633.e5.
1078 https://doi.org/10.1016/j.cmet.2024.06.001.

1079 57. Chang, A.M., Smith, M.J., Galecki, A.T., Bloem, C.J., and Halter, J.B. (2006). Impaired β-
1080 Cell Function in Human Aging: Response to Nicotinic Acid-Induced Insulin Resistance. J. Clin.
1081 Endocrinol. Metab. *91*, 3303–3309. https://doi.org/10.1210/jc.2006-0913.

1082 58. Ferrannini, E., Natali, A., Muscelli, E., Nilsson, P.M., Golay, A., Laakso, M., Beck-Nielsen,
1083 H., Mari, A., and Investigators, R. (2011). Natural history and physiological determinants of
1084 changes in glucose tolerance in a non-diabetic population: the RISC Study. Diabetologia *54*,
1085 1507–1516. https://doi.org/10.1007/s00125-011-2112-x.

1086 59. Ihm, S.-H., Matsumoto, I., Sawada, T., Nakano, M., Zhang, H.J., Ansite, J.D., Sutherland,
1087 D.E.R., and Hering, B.J. (2006). Effect of Donor Age on Function of Isolated Human Islets.
1088 Diabetes *55*, 1361–1368. https://doi.org/10.2337/db05-1333.

1089 60. Niclauss, N., Bosco, D., Morel, P., Demuylder-Mischler, S., Brault, C., Milliat-Guittard, L.,
1090 Colin, C., Parnaud, G., Muller, Y.D., Giovannoni, L., et al. (2011). Influence of Donor Age on
1091 Islet Isolation and Transplantation Outcome. Transplantation *91*, 360–366.
1092 https://doi.org/10.1097/tp.0b013e31820385e6.

1093 61. Lyon, J., Fox, J.E.M., Spigelman, A.F., Kim, R., Smith, N., O'Gorman, D., Kin, T., Shapiro,
1094 A.M.J., Rajotte, R.V., and MacDonald, P.E. (2016). Research-Focused Isolation of Human Islets
1095 From Donors With and Without Diabetes at the Alberta Diabetes Institute IsletCore.
1096 Endocrinology *157*, 560–569. https://doi.org/10.1210/en.2015-1562.

1097 62. Shrestha, S., Erikson, G., Lyon, J., Spigelman, A.F., Bautista, A., Fox, J.E.M., Santos, C.
1098 dos, Shokhirev, M., Cartailler, J.-P., Hetzer, M.W., et al. (2022). Aging compromises human islet
1099 beta cell function and identity by decreasing transcription factor activity and inducing ER stress.
1100 Sci Adv *8*, eabo3932. https://doi.org/10.1126/sciadv.abo3932.

1101 63. D'Aleo, V., Guerra, S.D., Gualtierotti, G., Filipponi, F., Boggi, U., Simone, P.D., Vistoli, F.,
1102 Prato, S.D., Marchetti, P., and Lupi, R. (2010). Functional and Survival Analysis of Isolated
1103 Human Islets. Transplant. Proc. *42*, 2250–2251.
1104 https://doi.org/10.1016/j.transproceed.2010.05.132.

1105 64. Ewald, J.D., Lu, Y., Ellis, C.E., Worton, J., Kolic, J., Sasaki, S., Zhang, D., Santos, T. dos,
1106 Spigelman, A.F., Bautista, A., et al. (2024). HumanIslets.com: Improving accessibility,

integration, and usability of human research islet data. Cell Metab. https://doi.org/10.1016/j.cmet.2024.09.001.

65. Walker, J.T., Saunders, D.C., Brissova, M., and Powers, A.C. (2021). The Human Islet: Mini-organ with Mega-impact. Endocr Rev *42*, bnab010-. https://doi.org/10.1210/endrev/bnab010.

66. Huang, J.L., Pourhosseinzadeh, M.S., Lee, S., Krämer, N., Guillen, J.V., Cinque, N.H., Aniceto, P., Momen, A.T., Koike, S., and Huising, M.O. (2024). Paracrine signalling by pancreatic δ cells determines the glycaemic set point in mice. Nat. Metab. *6*, 61–77. https://doi.org/10.1038/s42255-023-00944-2.

67. Zhang, J., McKenna, L.B., Bogue, C.W., and Kaestner, K.H. (2014). The diabetes gene Hhex maintains δ-cell differentiation and islet function. Genes Dev. *28*, 829–834. https://doi.org/10.1101/gad.235499.113.

68. Svendsen, B., and Holst, J.J. (2021). Paracrine regulation of somatostatin secretion by insulin and glucagon in mouse pancreatic islets. Diabetologia *64*, 142–151. https://doi.org/10.1007/s00125-020-05288-0.

69. Wessel, J., Chu, A.Y., Willems, S.M., Wang, S., Yaghootkar, H., Brody, J.A., Dauriz, M., Hivert, M.-F., Raghavan, S., Lipovich, L., et al. (2015). Low-frequency and rare exome chip variants associate with fasting glucose and type 2 diabetes susceptibility. Nat. Commun. *6*, 5897. https://doi.org/10.1038/ncomms6897.

70. Barg, S. (2003). Mechanisms of Exocytosis in Insulin-Secreting B-Cells and Glucagon-Secreting A-Cells. Pharmacol. Toxicol. *92*, 3–13. https://doi.org/10.1034/j.1600-0773.2003.920102.x.

71. Drigo, R.A. e, Jacob, S., García-Prieto, C.F., Zheng, X., Fukuda, M., Nhu, H.T.T., Stelmashenko, O., Peçanha, F.L.M., Rodriguez-Diaz, R., Bushong, E., et al. (2019). Structural basis for delta cell paracrine regulation in pancreatic islets. Nat. Commun. *10*, 3700. https://doi.org/10.1038/s41467-019-11517-x.

72. Perez-Frances, M., Bru-Tari, E., Cohrs, C., Abate, M.V., Gurp, L. van, Furuyama, K., Speier, S., Thorel, F., and Herrera, P.L. (2024). Regulated and adaptive in vivo insulin secretion from islets only containing β-cells. Nat. Metab. *6*, 1791–1806. https://doi.org/10.1038/s42255-024-01114-8.

73. Carlsson, P.-O., Hu, X., Scholz, H., Ingvast, S., Lundgren, T., Scholz, T., Eriksson, O., Liss, P., Yu, D., Deuse, T., et al. (2025). Survival of Transplanted Allogeneic Beta Cells with No Immunosuppression. N. Engl. J. Med. https://doi.org/10.1056/nejmoa2503822.

74. Reichman, T.W., Markmann, J.F., Odorico, J., Witkowski, P., Fung, J.J., Wijkstrom, M., Kandeel, F., Koning, E.J.P. de, Peters, A.L., Mathieu, C., et al. (2025). Stem Cell–Derived, Fully Differentiated Islets for Type 1 Diabetes. N. Engl. J. Med. https://doi.org/10.1056/nejmoa2506549.

1144 75. RIOS, P., MCGARRIGLE, J.J., LAMONICA, G., LI, Y., COOK, J., JOSHI, I., GHANI, S.,
1145 COOK, D., LOPEZ, D., NASIR, H., et al. (2024). 35-OR: Lantidra, First FDA-Approved Cellular
1146 Therapy to Treat Type 1 Diabetes. Diabetes *73*. https://doi.org/10.2337/db24-35-or.

1147 76. Shapiro, A.M., Lakey, J.R., Ryan, E.A., Korbutt, G.S., Toth, E., Warnock, G.L., Kneteman,
1148 N.M., and Rajotte, R.V. (2000). Islet transplantation in seven patients with type 1 diabetes
1149 mellitus using a glucocorticoid-free immunosuppressive regimen. New Engl J Medicine *343*, 230
1150 238. https://doi.org/10.1056/nejm200007273430401.

1151 77. Flatt, A.J., Matus, A.M., Gallop, R.J., Markmann, E., Dalton-Bakes, C., Peleckis, A.J., Liu,
1152 C., Naji, A., and Rickels, M.R. (2025). β-Cell Secretory Capacity Predicts Metabolic Outcomes
1153 Over 6 Years After Human Islet Transplantation. Diabetes.. *74*, 749–759.
1154 https://doi.org/10.2337/db24-0729.

1155 78. Buemi, A., Mourad, N.I., Ambroise, J., Hoton, D., Devresse, A., Darius, T., Kanaan, N.,
1156 Gianello, P., and Mourad, M. (2024). Donor- and isolation-related predictive factors of in vitro
1157 secretory function of cultured human islets. Front. Endocrinol. *15*, 1345351.
1158 https://doi.org/10.3389/fendo.2024.1345351.

1159 79. Shojania, K.G., Burton, E.C., McDonald, K.M., and Goldman, L. (2003). Changes in Rates of
1160 Autopsy-Detected Diagnostic Errors Over Time: A Systematic Review. JAMA *289*, 2849–2856.
1161 https://doi.org/10.1001/jama.289.21.2849.

Figure 1

A

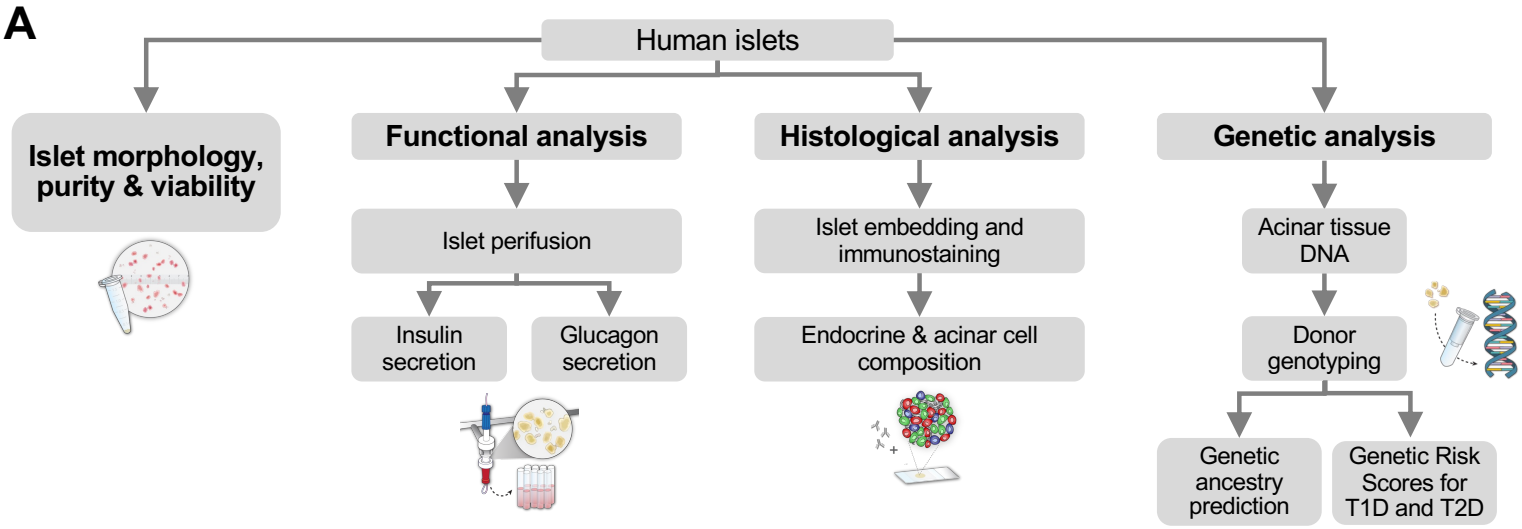

B

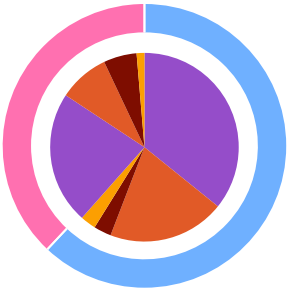

N = 299

Sex: Female Male

Reported race or ethnicity:
- Asian
- Black or African American
- Hispanic or Latino/a
- White

Reported race or ethnicity	Female (38%)				Male (62%)			
	% (N)	Age (yr)	BMI (kg/m²)	HbA1C (%)	% (N)	Age (yr)	BMI (kg/m²)	HbA1C (%)
Asian	3% (4)	49 ± 6 (43 – 57)	28.5 ± 4.8 (23.2 – 32.9)	5.5 ± 0.17 (5.3 – 5.6)	4% (8)	49 ± 13 (31 – 66)	26.5 ± 3.0 (21.6 – 29.9)	5.4 ± 0.33 (5.0 – 5.9)
Black or African American	15%** (17)	48 ± 14 (20 – 65)	30.6 ± 7.2 (18.2 – 47.6)	5.5 ± 0.42 (4.5 – 6.2)	5% (9)	47 ± 9 (37 – 62)	30.7 ± 6.9 (25.0 – 46.8)	5.5 ± 0.36 (5.0 – 6.1)
Hispanic or Latino/a	23% (26)	44 ± 12 (24 – 64)	30.0 ± 4.4 (22.9 – 38.7)	5.4 ± 0.42 (4.3 – 6.0)	33% (60)	40 ± 13 (15 – 62)	29.3 ± 4.7 (18.2 – 39.5)	5.5 ± 0.34 (4.5 – 6.1)
White	59% (68)	46 ± 10 (21 – 65)	28.9 ± 6.2 (17.6 – 45.5)	5.3 ± 0.43 (4.4 – 6.4)	58% (107)	45 ± 12 (17 – 68)	28.6 ± 4.8 (13.7 –40.7)	5.3 ± 0.39 (4.0 – 6.3)
Combined	38% (115)	46 ± 11 (20 – 65)	29.4 ± 5.9 (17.6 – 47.6)	5.3 ± 0.42 (4.3 – 6.4)	62% (184)	43 ± 13 (15 – 68)	28.8 ± 4.9 (13.7 – 46.8)	5.4 ± 0.37 (4.0 – 6.3)

Values reported as mean ± SD (range)

C

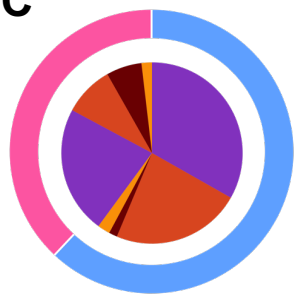

N = 268

Sex: Female Male

Primary predicted ancestry:
- East Asian
- African
- Admixed American
- European

Primary predicted ancestry	Female (40%)				Male (60%)			
	% (N)	Age (yr)	BMI (kg/m²)	HbA1C (%)	% (N)	Age (yr)	BMI (kg/m²)	HbA1C (%)
East Asian	5% (5)	48.2 ± 4 (43 – 57)	29.0 ± 4.3 (23.2 – 32.9)	5.4 ± 0.2 (5.2 – 5.6)	4% (6)	51.3 ± 15 (31 – 66)	25.9 ± 3.3 (21.6 – 29.9)	5.5 ± 0.3 (5.1 – 5.9)
African	16%*** (17)	48.5 ± 14 (20 – 65)	30.6 ± 7.2 (18.2 – 47.6)	5.5 ± 0.4 (4.5 – 6.2)	2.5% (4)	46.5 ± 9 (37 – 58)	32.4 ± 9.8 (25 – 46.8)	5.7 ± 0.4 (5.1 – 6.1)
Admixed American	22%** (24)	44.9 ± 12 (24 – 61)	29.6 ± 4.7 (22 – 38.7)	5.4 ± 0.4 (4.3 – 5.9)	38.5% (62)	39.6 ± 13 (15 – 62)	29.4 ± 4.8 (18.2 – 40)	5.4 ± 0.3 (4.5 – 6.1)
European	57% (61)	46.4 ± 10 (21 – 65)	28.9 ± 6.4 (17.6 – 45.5)	5.3 ± 0.4 (4.4 – 6.4)	55% (89)	46.0 ± 12 (18 – 68)	28.4 ± 5.0 (13.7 – 40.7)	5.3 ± 0.4 (4.0 – 6.3)
Combined	40% (107)	46 ± 11 (20 – 65)	29.4 ± 6.1 (17.6 – 47.6)	5.4 ± 0.42 (4.3 – 6.4)	60% (161)	44 ± 13 (15 – 68)	28.8 ± 5.0 (13.7 – 46.8)	5.4 ± 0.37 (4.0 – 6.3)

Values reported as mean ± SD (range)

Figure 2

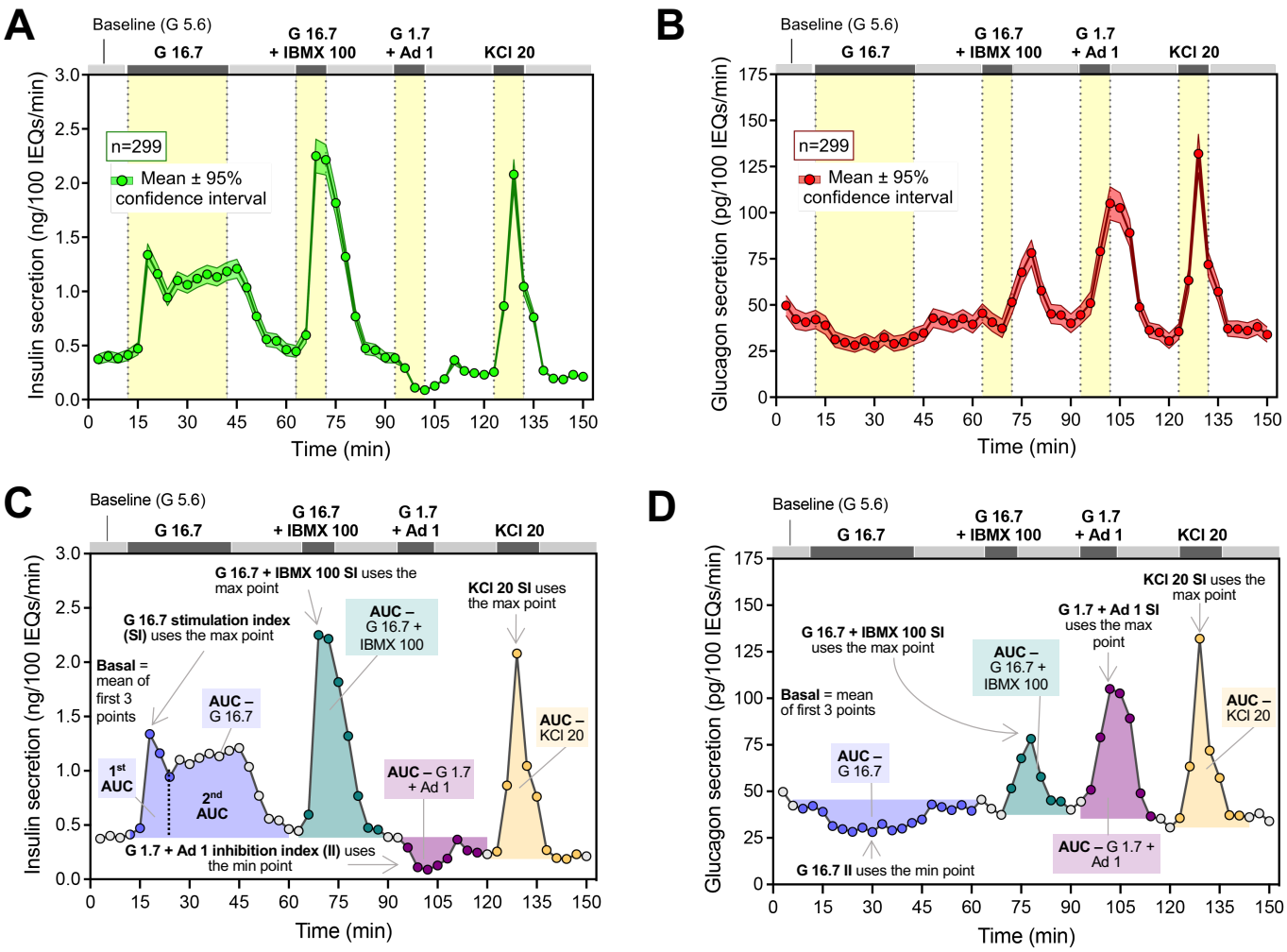

Secretagogue	Purpose	Time (start – end)	Duration (min)	Baseline (t=)	AUC (range)	SI / II (range)
Basal glucose	Basal secretion	0-12	12	3-9	-	-
High glucose	Glucose-stimulated insulin secretion	12-42	30	3-6 (SI) 3-12 (16.7 1st AUC) 9,60 (16.7 AUC)	3-24 (16.7 1st) 9-60 (16.7)	9-27
Basal glucose	-	42-63	21	-	-	-
High glucose + IBMX	cAMP signaling potentiation	63-72	9	60-63 (SI) 63,90 (AUC)	63-90	63-90
Basal glucose	-	72-93	21	-	-	-
Low glucose + adrenaline	Insulin inhibition	93-102	9	90-93 (II) 93,120 (AUC)	93-120	90-108
Basal glucose	-	102-123	21	-	-	-
Glucose + KCl	Membrane depolarization	123-132	9	117-120 (SI) 120,150 (AUC)	120-150	120-150
Basal glucose	-	132-150	18	-	-	-

Secretagogue	Purpose	Time (start – end)	Duration (min)	Baseline (t=)	AUC (range)	SI / II (range)
Basal glucose	Basal secretion	0-12	12	3-6	-	-
High glucose	Glucagon inhibition	12-42	30	3-6 (II) 3-6 (AUC)	3-63	3-42
Basal glucose	-	42-63	21	-	-	-
High glucose + IBMX	cAMP signaling potentiation	63-72	9	60-63 (SI) 69,90 (AUC)	69-90	63-90
Basal glucose	-	72-93	21	-	-	-
Low glucose + adrenaline	Glucagon secretion	93-102	9	90-93 (SI) 93,117 (AUC)	93-117	93-117
Basal glucose	-	102-123	21	-	-	-
Glucose + KCl	Membrane depolarization	123-132	9	117-120 (SI) 120,144 (AUC)	120-144	120-144
Basal glucose	-	132-150	18	-	-	-

G 16.7 2nd AUC was calculated by subtracting the G 16.7 1st AUC from the total G 16.7 AUC.

Figure 3

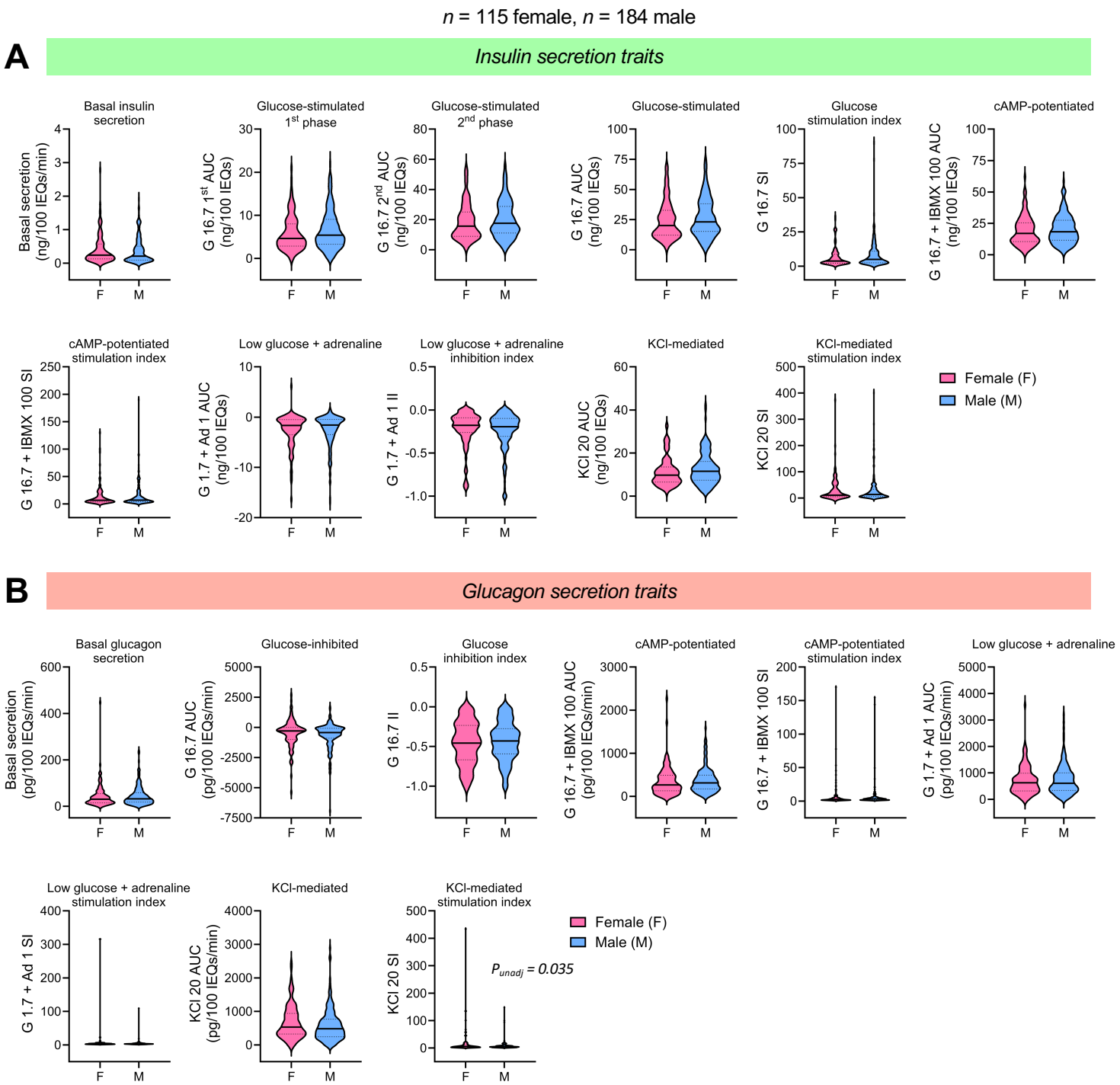
n = 115 female, n = 184 male
A
Insulin secretion traits
Basal insulin secretion
Basal secretion (ng/100 IEQs/min)
Glucose-stimulated 1st phase
G 16.7 1st AUC (ng/100 IEQs)
Glucose-stimulated 2nd phase
G 16.7 2nd AUC (ng/100 IEQs)
Glucose-stimulated
G 16.7 AUC (ng/100 IEQs)
Glucose stimulation index
G 16.7 SI
cAMP-potentiated
G 16.7 + IBMX 100 AUC (ng/100 IEQs)
cAMP-potentiated stimulation index
G 16.7 + IBMX 100 SI
Low glucose + adrenaline
G 1.7 + Ad 1 AUC (ng/100 IEQs)
Low glucose + adrenaline inhibition index
G 1.7 + Ad 1 II
KCl-mediated
KCl 20 AUC (ng/100 IEQs)
KCl-mediated stimulation index
KCl 20 SI
F
M
Female (F)
Male (M)
B
Glucagon secretion traits
Basal glucagon secretion
Basal secretion (pg/100 IEQs/min)
Glucose-inhibited
G 16.7 AUC (pg/100 IEQs/min)
Glucose inhibition index
G 16.7 II
cAMP-potentiated
G 16.7 + IBMX 100 AUC (pg/100 IEQs/min)
cAMP-potentiated stimulation index
G 16.7 + IBMX 100 SI
Low glucose + adrenaline
G 1.7 + Ad 1 AUC (pg/100 IEQs/min)
Low glucose + adrenaline stimulation index
G 1.7 + Ad 1 SI
KCl-mediated
KCl 20 AUC (pg/100 IEQs/min)
KCl-mediated stimulation index
KCl 20 SI
Female (F)
Male (M)
P_{unadj} = 0.035

Figure 4

n = 12 Asian, *n* = 26 Black or African American, *n* = 86 Hispanic or Latino/a, *n* = 175 White

A

Insulin secretion traits

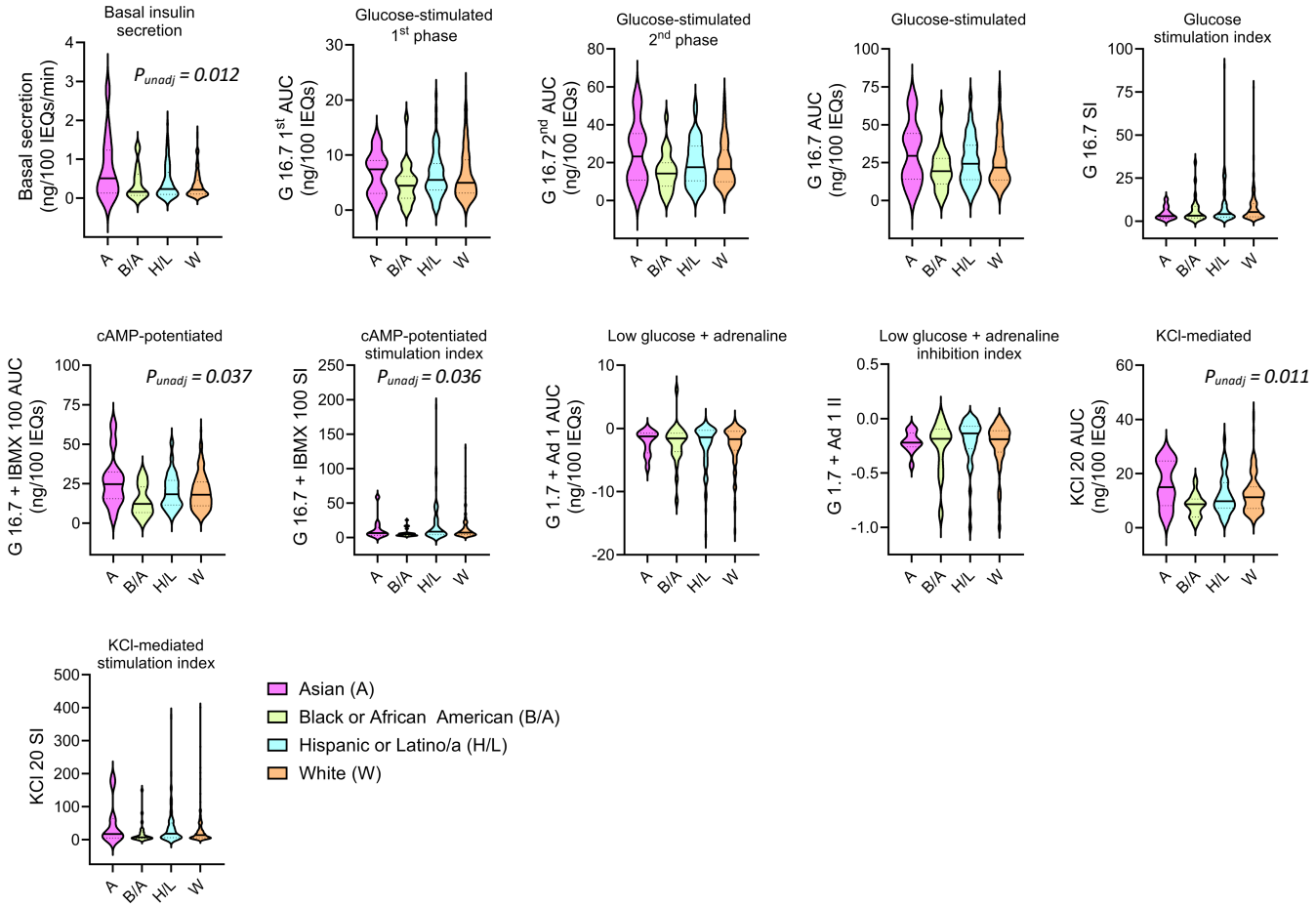

B

Glucagon secretion traits

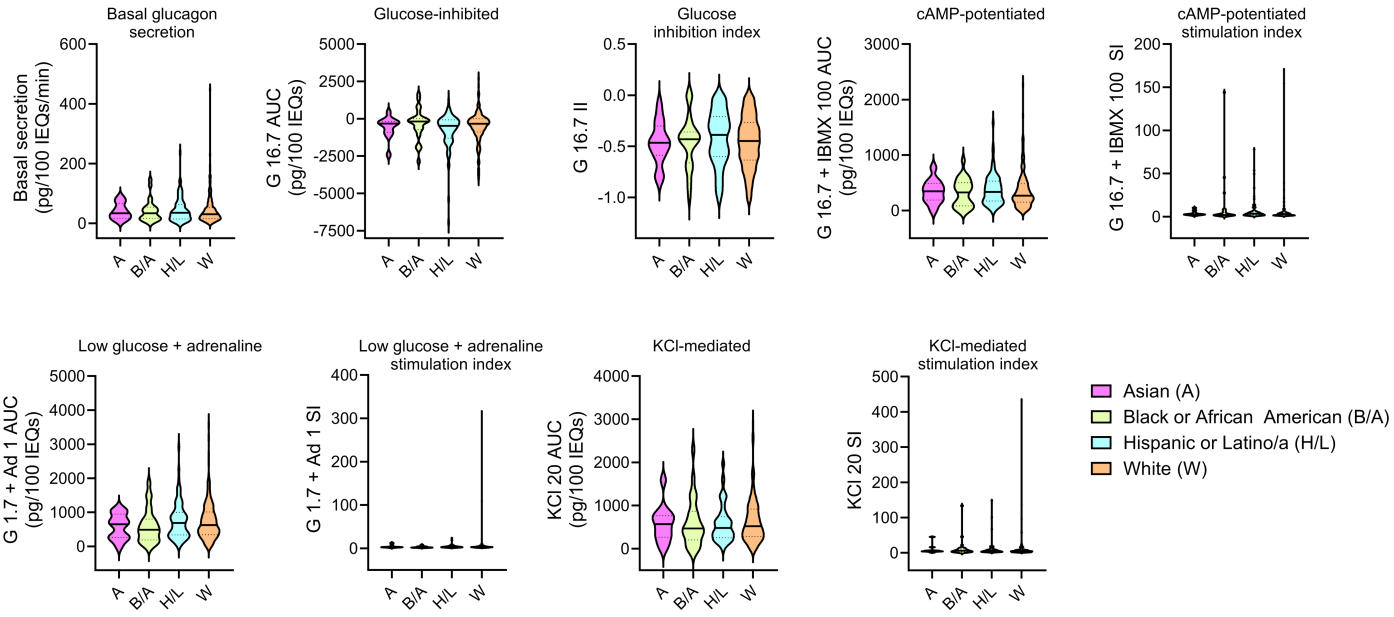

Figure 5

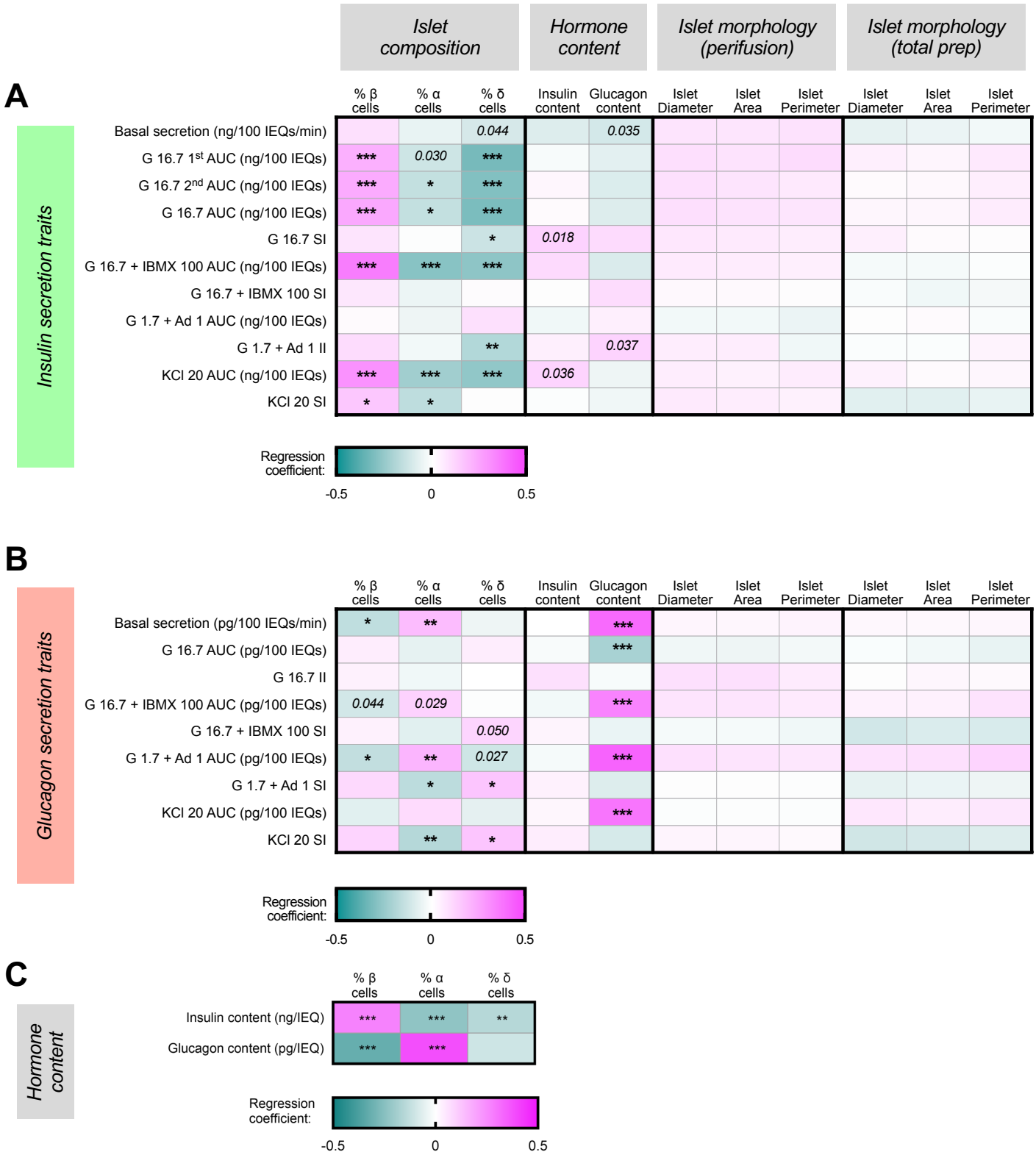
A
Islet composition
Hormone content
Islet morphology (perifusion)
Islet morphology (total prep)
% β cells
% α cells
% δ cells
Insulin content
Glucagon content
Islet Diameter
Islet Area
Islet Perimeter
Islet Diameter
Islet Area
Islet Perimeter
Insulin secretion traits
Basal secretion (ng/100 IEQs/min)
G 16.7 1st AUC (ng/100 IEQs)
G 16.7 2nd AUC (ng/100 IEQs)
G 16.7 AUC (ng/100 IEQs)
G 16.7 SI
G 16.7 + IBMX 100 AUC (ng/100 IEQs)
G 16.7 + IBMX 100 SI
G 1.7 + Ad 1 AUC (ng/100 IEQs)
G 1.7 + Ad 1 II
KCl 20 AUC (ng/100 IEQs)
KCl 20 SI
Regression coefficient:
-0.5
0
0.5
B
Glucagon secretion traits
Basal secretion (pg/100 IEQs/min)
G 16.7 AUC (pg/100 IEQs)
G 16.7 II
G 16.7 + IBMX 100 AUC (pg/100 IEQs)
G 16.7 + IBMX 100 SI
G 1.7 + Ad 1 AUC (pg/100 IEQs)
G 1.7 + Ad 1 SI
KCl 20 AUC (pg/100 IEQs)
KCl 20 SI
Regression coefficient:
-0.5
0
0.5
C
Hormone content
% β cells
% α cells
% δ cells
Insulin content (ng/IEQ)
Glucagon content (pg/IEQ)
Regression coefficient:
-0.5
0
0.5

Figure 6

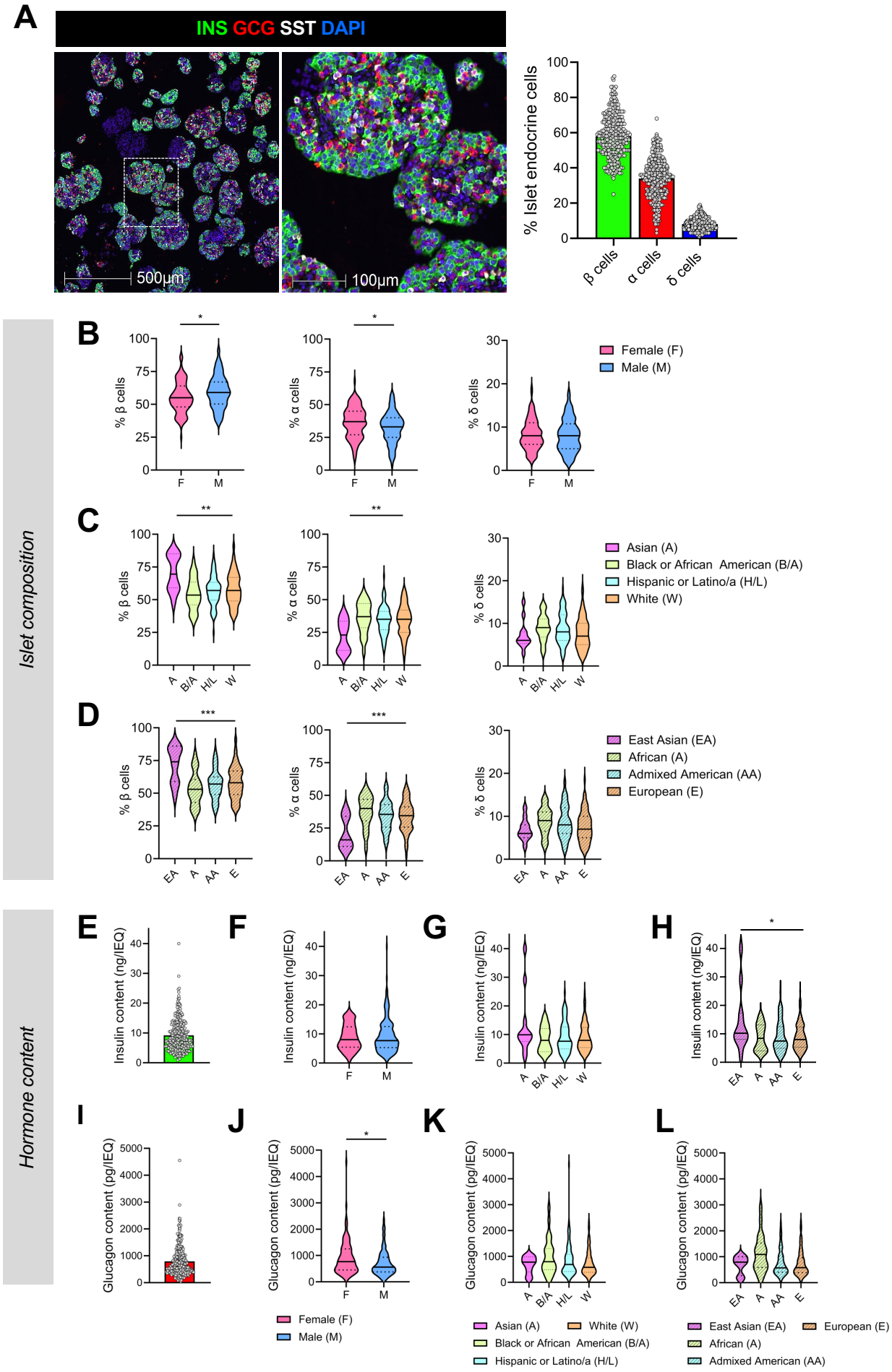
A
INS GCG SST DAPI
500µm
100µm
% Islet endocrine cells
β cells
α cells
δ cells
Islet composition
B
% β cells
% α cells
% δ cells
F
M
Female (F)
Male (M)
C
A
B/A
H/L
W
Asian (A)
Black or African American (B/A)
Hispanic or Latino/a (H/L)
White (W)
D
EA
AA
E
East Asian (EA)
African (A)
Admixed American (AA)
European (E)
Hormone content
E
F
G
H
Insulin content (ng/IEQ)
I
J
K
L
Glucagon content (pg/IEQ)

Figure 7

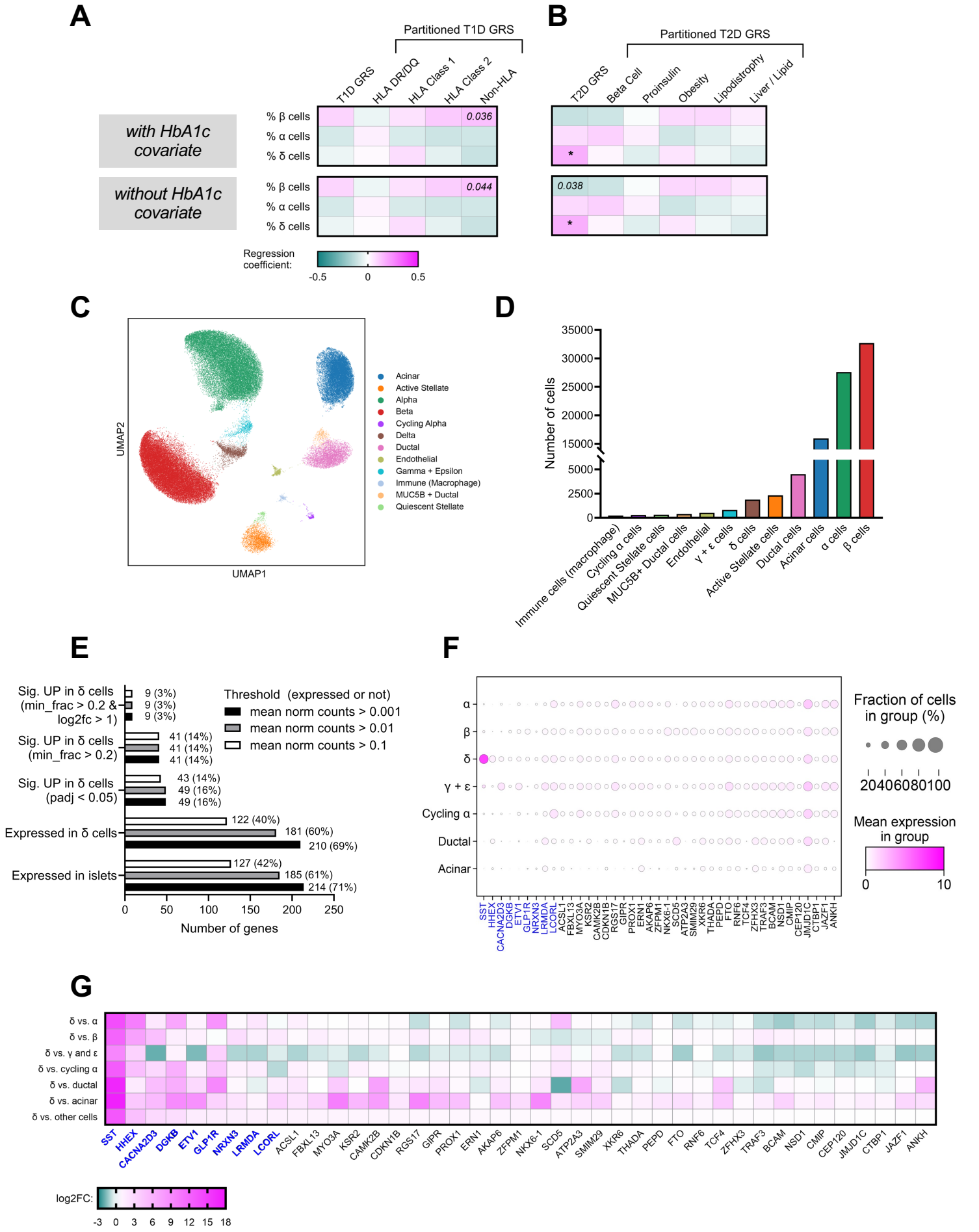
A
Partitioned T1D GRS
T1D GRS
HLA DR/DQ
HLA Class 1
HLA Class 2
Non-HLA
with HbA1c covariate
without HbA1c covariate
% β cells
% α cells
% δ cells
0.036
0.044
Regression coefficient:
-0.5
0
0.5
B
Partitioned T2D GRS
T2D GRS
Beta Cell
Proinsulin
Obesity
Lipodistrophy
Liver / Lipid
0.038
*
C
UMAP2
UMAP1
Acinar
Active Stellate
Alpha
Beta
Cycling Alpha
Delta
Ductal
Endothelial
Gamma + Epsilon
Immune (Macrophage)
MUC5B + Ductal
Quiescent Stellate
D
Number of cells
35000
30000
25000
20000
15000
5000
2500
0
Immune cells (macrophage)
Cycling α cells
Quiescent Stellate cells
MUC5B+ Ductal cells
Endothelial
γ + ε cells
δ cells
Active Stellate cells
Ductal cells
Acinar cells
α cells
β cells
E
Sig. UP in δ cells (min_frac > 0.2 & log2fc > 1)
9 (3%)
Sig. UP in δ cells (min_frac > 0.2)
41 (14%)
Sig. UP in δ cells (padj < 0.05)
43 (14%)
49 (16%)
Expressed in δ cells
122 (40%)
181 (60%)
210 (69%)
Expressed in islets
127 (42%)
185 (61%)
214 (71%)
Threshold (expressed or not)
mean norm counts > 0.001
mean norm counts > 0.01
mean norm counts > 0.1
0
50
100
150
200
250
Number of genes
F
α
β
δ
γ + ε
Cycling α
Ductal
Acinar
SST
HHEX
CACNA2D3
DGKB
ETV1
GLP1R
NRXN3
LRMDA
LCORL
ACSL1
FBXL13
MYO3A
KSR2
CAMK2B
CDKN1B
RGS17
GIPR
PROX1
ERN1
AKAP6
ZFPM1
NKX6-1
SCD5
ATP2A3
SMIM29
XKR6
THADA
PEPD
FTO
RNF6
TCF4
ZFHX3
TRAF3
BCAM
NSD1
CMIP
CEP120
JMJD1C
CTBP1
JAZF1
ANKH
Fraction of cells in group (%)
20
40
60
80
100
Mean expression in group
0
10
G
δ vs. α
δ vs. β
δ vs. γ and ε
δ vs. cycling α
δ vs. ductal
δ vs. acinar
δ vs. other cells
log2FC:
-3
0
3
6
9
12
15
18